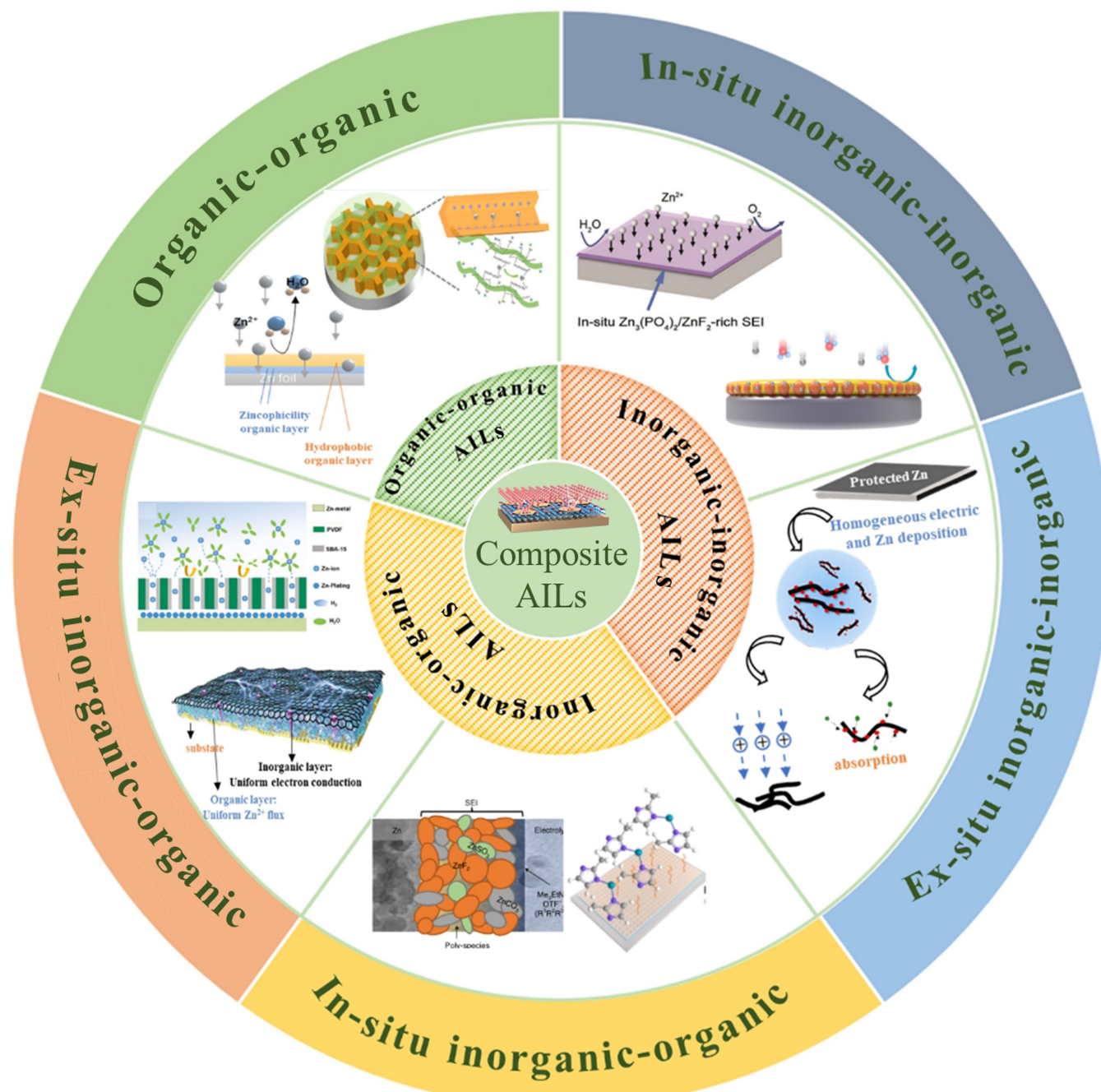


Special Collection

# Functional Oriented Design of Composite Artificial Interface Layers Towards Stable Zinc Anodes In Aqueous Zinc-ion Batteries

Xiaoyu Zhang<sup>+</sup>,<sup>[a]</sup> Weihua Jin<sup>+</sup>,<sup>[a]</sup> Min Liu<sup>+</sup>,<sup>[a]</sup> Yong Zhao,<sup>\*[b]</sup> and Peng Zhang<sup>\*[a]</sup>



Rechargeable aqueous zinc-ion batteries (AZIBs) with metallic Zn anodes have been regarded as attractive candidates for large-scale energy storage systems due to their affordability, safety, and high energy density. However, the practical implementation of rechargeable AZIBs is still hampered severely by the poor electrochemical stability and reversibility of Zn anodes, stemming from uncontrolled dendrite growth and rampant side reactions. Due to the versatility of different components in the composite artificial interface layer (AIL), great efforts on multifunctional AILs have recently been devoted to Zn anode protection for designing durable and

stable AZIBs. This review first presents a comprehensive and timely summarization on the origin and mechanism of dendrite growth and side reactions, followed by the systematic summarization of five protection mechanisms/functions of the AILs. Next, recent advances are discussed in the manner of a correlation between the combined materials/structures in composite AILs and their synergistic functionality, highlighting the critical role of functional orientation design of the composite AILs towards stable Zn anodes. Finally, perspectives and suggestions are provided for designing highly effective multifunctional composite AILs towards Zn anodes for AZIBs.

## 1. Introduction

The development of clean and renewable energy has entered the fast lane due to the concern of environmental aggravation and the continuous depletion of fossil fuels.<sup>[1]</sup> However, one of the critical issues is that sustainable energy resources (such as solar, wind, and tides) have difficult in being primitively utilized owing to their discontinuous, uncontrollable, and unstable power generation.<sup>[2]</sup> Developing available energy storage systems based on renewable energy has been recognized as a scientific approach to counteract decreasing fossil fuels reserves and increasing environmental issues.<sup>[3]</sup> Hence, the development of secondary batteries for energy redistribution is underscored by both academic and industrial circles.<sup>[4–5]</sup> Recently, the researches of exploring the batteries with aqueous electrolytes such as metallic sodium,<sup>[6]</sup> aluminum,<sup>[7]</sup> magnesium<sup>[8]</sup> and zinc,<sup>[9]</sup> have accelerated increasingly due to their high security and affordability. Among plentiful candidates, aqueous zinc ion batteries (AZIBs) employing Zn metal as the anode, Zn-intercalating compounds as the cathode (Prussian blue analogs),<sup>[10]</sup> and neutral or subacidity solution as electrolyte. AZIBs embrace promising potential because of high theoretical capacity ( $5855 \text{ mAh cm}^{-2}$ ), suitable working potential ( $-0.76 \text{ V}$  vs. SHE), considerable resources of Zn anode and high flame resistance.<sup>[11]</sup> Thereby, AZIBs are suitable for large-scale implementation applications in the post-lithium-ion batteries era.

However, there still exist unresolved constrictions in the electrode and electrolyte of AZIBs.<sup>[12–14]</sup> The performance and lifespan of AZIBs are dramatically influenced by the stabilization of Zn anodes. On the one hand, the practical application of stable AZIBs is limited by dendrite formation on the anode surface. Zn dendrites are generally associated with uneven Zn deposition during  $\text{Zn}^{2+}$  plating processes, which is an actually unavoidable phenomenon owing to the minienvironment on the anode-electrolyte interfaces.<sup>[15,16]</sup> Serious Zn dendrites may cause low anode reversibility and even ultimately puncture the spectator, which would lead to battery short circuit.<sup>[17,18]</sup> The degree of dendrite formation is affected by various factors, including polarization and current density.<sup>[19]</sup> On the other hand, the accompanying side reactions and byproducts accumulation on the Zn anode also have a significant impact on the stability of the Zn anode. The side reactions usually include the electrochemical hydrogen evolution reaction (HER) causing a cell to expand in volume and the corrosion reaction, spontaneously reacting with electrolyte and usually concomitant with HER, causing the chemical formation of byproducts. Therefore, with the battery operation, the battery deterioration, in terms of reduced the Coulomb efficiency (CE), cell expansion and increased  $\text{Zn}^{2+}$  diffusion impedance, is inevitable.<sup>[20]</sup> At present, numerous strategies have been proposed to stabilize Zn anode by reducing Zn dendrites and inhibiting side reactions, such as regulating and controlling the structure of Zn anodes,<sup>[21–24]</sup> optimizing current collectors,<sup>[25–27]</sup> modifying separators,<sup>[28–29]</sup> introducing artificial interface layers (AILs) on the anode surface,<sup>[30,31]</sup> adding electrolyte additives to electrolytes,<sup>[32–33]</sup> and employing eutectic electrolyte solutions (Figure 1).<sup>[34–36]</sup> Among these strategies, introducing AILs attract much attention due to the features of comprehensive functions including homogenizing nucleation sites, guiding (002) plane growth, aiding ion desolvation, offering  $\text{Zn}^{2+}$  transportation channels, and accelerating mass transfer.

AILs were initially used in lithium-ion batteries to stabilize lithium anode. In the field of AZIBs, extensive studies have revealed that AILs could effectively protect Zn anode from corrosion reaction as well as relieve the formation of Zn dendrite.<sup>[37–39]</sup> Normally, the Zn electroplating process takes place between the interface layer and the metal, which is related to the ion diffusion rate and the ability of electron migration. Electrons cannot be migrated in the electrical insulated AILs while  $\text{Zn}^{2+}$  can be freely transported through

[a] X. Zhang,<sup>+</sup> W. Jin,<sup>+</sup> M. Liu,<sup>+</sup> Dr. P. Zhang

Department of Chemistry

College of Science Northeastern University Shenyang  
110819, Liaoning (PR China)

E-mail: zhangpeng1@mail.neu.edu.cn

[b] Prof. Y. Zhao

Key Lab for Special Functional Materials of Ministry of Education  
National & Local Joint Engineering Research Center for High-efficiency  
Display and Lighting Technology

School of Materials Science and Engineering

Collaborative Innovation Center of Nano Functional Materials and

Applications

Henan University

Kaifeng 475004 (PR China)

E-mail: zhaoyp@henu.edu.cn

[+] These authors contributed equally to this work.

An invited contribution to a Special Collection on Young Scientists in Battery Research



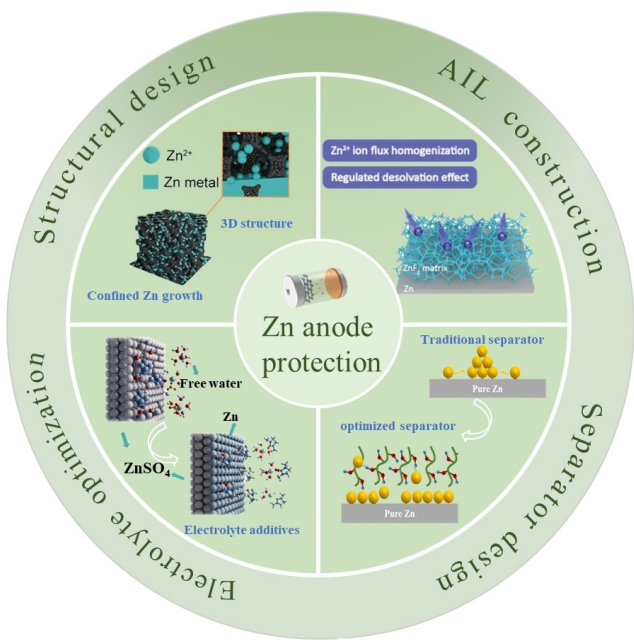


**Figure 1.** Schematic illustration of strategies for stabilizing Zn anode. The inserted graphics are reproduced with permission from ref. [61–64].

AILs and tend to deposit below the AILs. On the contrary, when electron conductive AILs used, Zn could be deposited on the top of the layers. Once the interface layer was covered by Zn plating, Zn will happen a series of side reactions with the electrolyte.<sup>[40]</sup> Therefore, numerous AILs are designed to be electrically insulative to avoid the electrodeposition of Zn on the top surface of AIL. Simultaneously, from the view of decreasing the locally surface current density of Zn anode, some conductive AILs are also designed with a three-dimensional (3D) framework to confine the Zn deposition within the framework through modulating the zincophile affinity. Generally, it is the ultimate aim to achieve fast Zn deposition, inhibit Zn dendrite formation and isolate Zn anode from electrolyte for the ideal design of AILs.<sup>[41]</sup> In order to adjust the requirements of commercialization and realizing the comprehensive functions of the AILs, the requiring characters are as follows: 1) Carrying sufficient mechanical strength to block tough dendrites.<sup>[42]</sup> 2) Carrying stable chemical properties to prevent interfacial side reaction between electrolyte and Zn electrode.<sup>[43]</sup> 3) Providing uniform Zn nucleation sites to increase Zn affinity.<sup>[44]</sup> 4) Carrying high ionic conductivity to accelerate the mass transfer kinetics of Zn ion.

Up to now, vary of materials have been employed to construct AILs to stable Zn anode, mainly including inorganic materials (metal matrix materials,<sup>[45–48]</sup> carbon-based materials<sup>[49–52]</sup>), organic materials (polymers,<sup>[53,54]</sup> metal organic

Xiaoyu Zhang received her Bachelor's degree from Shenyang Agricultural University in 2022. She is currently a postgraduate supervised by Dr. Peng Zhang in Department of Chemistry, Northeastern University. Her research interests focus on the design of high-performance electrolytes and electrode materials for aqueous zinc-ion batteries.

Weihua Jin received his B.S. degree in chemical engineering from University of Science and Technology Liaoning in 2022. He is currently a postgraduate supervised by Dr. Peng Zhang in Department of Chemistry, Northeastern University. His research interests focus on high-performance lithium sulphur batteries.

Yong Zhao is a professor at School of Materials Science and Engineering, Henan University, where his interests are design and construction of novel electrolytes and materials for high specific energy batteries as well as the exploration of electrode reaction mechanism. He received his PhD from the Institute of Chemistry, Chinese Academy of Sciences, in 2008 under the supervision of Prof. Lei Jiang, followed by a period working as a postdoctoral fellow with Prof. Kazuhito Hashimoto at the University of Tokyo (2008–2015).

Peng Zhang is an associate professor in Department of Chemistry, College of Science, Northeastern University. His research interests focus on interface stability based on the energy materials and electrolytes system. He received his PhD from Lanzhou Institute of Chemical Physics, Chinese Academy of Sciences, in 2016, followed by a working and postdoctoral experience at Henan University and Wuhan University/Southern University of Science and Technology, respectively.

Min Liu is an experimentalist in Chemical Laboratory, College of Science, Northeastern University. She worked at Northeastern University since 2016. She is mainly responsible for tests of valuable instruments, TEM, SEM, XRD, etc.

frameworks,<sup>[55]</sup> organic molecule monolayers<sup>[56]</sup> and covalent organic frameworks<sup>[57]</sup>, as well as their composites. Single-component AILs normally cannot satisfy all the four requirements as mentioned above and thus usually result in undesirable protective effect towards Zn anode. One AIL may encounter the inferior zincophilicity, the weak mechanical rigidity, or the strong hydrophilicity, and then lead to the falling off of the interface layer, the crack of the interface layer, and the hydrogen evolution, respectively.<sup>[4]</sup> For example, Carbon nanofibers (CNFs) are proposed to homogenize the charge distribution and hinder Zn dendrite growth during Zn plating due to their high conductivity, porosity and chemically/electrochemically stability. Nevertheless, the low affinity of CNFs towards Zn, like other pristine carbon substrates, typically results in sluggish kinetics for Zn deposition and the following high battery polarization.<sup>[58]</sup> Simultaneously, the generally low Zn<sup>2+</sup> conductivity of CNFs limits the cycling performance of the anode at high current.<sup>[59]</sup> Yang and coworkers fabricated a composite coating layer incorporating Cu with porous and conductive CNFs (Cu-CNFs) to stabilize Zn anodes in virtue of the high zincophile affinity of Cu. The composite Cu-CNFs AIL combined both advantages of protective function of CNFs and Cu. The porous CNFs with a large specific surface area reduced local current density and homogenized the distribution of electric fields while the modified Cu nanoparticles on CNFs greatly reduce the nucleation overpotential of Zn.<sup>[60]</sup> This kind of structural and zincophilic composite AILs are endowed with polyfunctionality to overcome the issues encountered by a single-component AIL.

In this review, we present a comprehensive summarization of multifunctional composite AILs to stabilize Zn metal anode for AZIBs. We will start with the discussion of the origin of dendrite formation and side reactions, followed by analyzing their fundamental mechanisms. Next, the mechanisms of AILs to inhibit dendrite growth and side reactions will be categorized from severing as physical isolation barrier, homogenizing the Zn<sup>2+</sup> flux, reducing nucleation barrier, inducing uniformizing electrical field, regulating the solvation structure of Zn<sup>2+</sup>. The main context discusses the state-of-the-art composite AILs toward improve Zn anode from the perspective of understanding and establishing the correlation between specific materials/structures and their functionality within composite AILs. In this section, three parts are divided according to the material type, including inorganic-organic materials, inorganic-inorganic materials and organic-organic materials. We expect this review will promote a deeper insight into the exploration and optimization of the Zn metal anode for the practical application of AZIBs.

## 2. Challenges and the Mechanisms of AILs to Stabilize Zn Anodes

Zn metal has been widely deployed to the anode materials of ZIBs by far. Despite its various merits, it still suffers from some detrimental bottlenecks which impede the lifespan of AZIBs. In

this study, dendrite growth was analyzed in terms of nucleation, polarization, Zn<sup>2+</sup> transportation, electric field, and side reactions on the anode surface were discussed in terms of HER and by-product generation. Up to now, it is acknowledged that constructing AILs is an effective strategy to prevent these detrimental bottlenecks due to their multiply functions on Zn anode, including physical isolation barrier, homogenizing the Zn<sup>2+</sup> flux, optimizing nucleation barrier, modulating electrical field, regulating the solvation structure of Zn<sup>2+</sup>. These factors are specifically analyzed as follows.

### 2.1. Zn dendrites

The dendrite formation is an inherent characteristic of Zn metal. In general, non-uniform electrochemical reactions would occur owing to instable/inhomogenous microenvironment (cation and electric field distribution, and evenness of anodes) at Zn anode/aqueous electrolyte interface, resulting in the faster growth of Zn<sup>2+</sup> at certain deposition sites, namely dendritic seeds. Following that, Zn<sup>2+</sup> diffuses and accumulates at pre-existing nucleation seeds. Some protrusions may be subjected to higher electrical intensity and higher Zn<sup>2+</sup> ion concentration, which is called "tip effect" leading to fast dendrite growth.<sup>[65]</sup> More specifically, the deposited Zn tends to form hexagonal platelets to reduce the thermodynamic free energy. In the process of cycling, the Zn platelets in these prominent parts are nonuniformly distributed, even grow in random way. They subsequently develop into quite large irregular dendrites piercing the separators.<sup>[66]</sup>

The initial time of dendritic formation is described by "Sand's time" in dilute solution. For the Zn metal anode in the aqueous electrolyte, the cation will be rapidly consumed, and then its concentration near the electrode is expected to reduce to zero at a certain moment. Subsequently, a large number of Zn<sup>2+</sup> is absorbed adjacent to anode surface by a strong electronegative electric field and then electrodeposited on the initial hump position in a short time, causing the growth of dendrites.<sup>[67]</sup> This behavior is known as "Sand's behavior", and this time is called Sand's time:

$$t_{\text{sand}} = \pi D_l \left[ \frac{nFC_l^0}{2i} \right]^2 \quad (1)$$

where  $D_l$  is the diffusion coefficient electrolyte "liquid" phase,  $n$  is the number of transferred electrons,  $F$  is the Faraday constant, and  $C_l^0$  is the initial concentration of cation,  $i$  is current density. A large  $t_{\text{sand}}$  benefits the free-dendrites of realization, which can be achieved by increasing  $C_l^0$ , decreasing  $i$  or employing large  $D_l$  electrolyte from Equation (1).

As a notorious problem, the formation of Zn dendrites limits the practical application of Zn metal anodes in neutral or slightly acidic AZIBs. Uneven Zn deposition is well established as a chief reason for Zn dendrites during the Zn plating/stripping processes, leading to an uneven surface.<sup>[68]</sup> The inhomogeneous electrode surface may result in an inhomogeneous electric field and swelling anode, aggravating dendrite

growth and capacity decay.<sup>[69]</sup> On the other hand, asymptotic dead Zn on the electrode formed by the separation of the dendrite root from the Zn anode is no longer as an active component, which ultimately leads to the low CE and reduced battery cycling lifespan.<sup>[70]</sup> Additionally, the uncontrolled Zn dendrites may continuously grow and puncture the separators resulting in eventually short circuit of the batteries. There are many factors affecting the complex process of Zn dendrite formation, such as the nucleation, the Zn<sup>2+</sup> diffusion, interfacial electric field, current density, concentration gradient, capacity, and even the structure of anode.<sup>[66]</sup>

### 2.1.1. Nucleation

The growth of Zn begins with nucleation process. Four models are proposed to explain the nucleation process, namely the two-dimensional (2D) nucleation model including 2D instantaneous nucleation<sup>[71]</sup> and 2D progressive nucleation<sup>[72]</sup> and the 3D nucleation model<sup>[73]</sup> including 3D instantaneous nucleation (3DI) and 3D progressive nucleation<sup>[44]</sup> (3DP). The 2D nucleation that enters the lattice page by diffusion of adsorbed atoms is different from the 3D nucleation controlled by volume diffusion. 2D nucleation is not instrumental in realizing of dendrite-free deposition, because the adsorbed atoms are prone to diffuse to the lowest position of the energy barrier, so that minimize the surface energy. This energy-preferred deposition mode will accelerate the local accumulation of Zn and result in dendrite formation. On the contrary, 3D nucleation is more conducive to achieving uniform Zn deposition without dendrite. In addition, compared with 3D instantaneous deposition, 3D asymptotic deposition can be more conducive to promote uniform Zn deposition because of the continuous activation of new nucleation sites.<sup>[4]</sup>

It is widely accepted that Zn nucleation and subsequent growth need to overcome the nucleation barrier.<sup>[74–75]</sup> The nucleation barrier is usually defined as the difference between the tip potential and the subsequent stable potential, the thermodynamic energy required to form a Zn nucleus. In principle, these two potentials difference should be as small as possible to reduce resistance during nucleation, which is beneficial to improving Zn plating quality and reducing energy consumption.<sup>[2]</sup> Simultaneously, enhancing the nucleation barrier to some extent has also been proved to facilitate the dense and even nucleation behavior. These two viewpoints are not contradictory because it is closely related to the property of the designed active sites for Zn deposition, such as active sites density and their affinity towards Zn. Generally, during electro-deposition, the orientation of Zn deposition is easily affected by electroplating conditions, such as the flatness of deposited substrate, the uniformity of electric field at the substrate-electrolyte interface, and the zincophilicity of substrate.<sup>[1]</sup> The nucleation process plays an important role in the subsequent Zn growth. The relative balanced electric field at the interface can be influenced by random Zn distribution at the nucleation process. Therefore, a flat surface with uniform nucleation sites can minimize the inhomogeneity of Zn growth.

### 2.1.2. Polarization

From a kinetics perspective, the deposition of Zn is easily affected by the polarization process. When there is a current flowing through the electrodes, it will be polarized due to the existences of different types of resistances, causing the delay of capacity. Three of these resistances are considered to play significant roles: ohmic resistance caused by solid-phase electron transport, liquid-phase ionic transport resistance, and charge transfer resistance at the interface between electrode and electrolyte.<sup>[76]</sup> Zn ions usually exist in the form of one Zn ion surrounded by six adjacent molecules in aqueous electrolyte. The increase of ionic radius increases the transport barrier of Zn ions.<sup>[77]</sup> Zn<sup>2+</sup> liquid-phase transport is slower in comparison to the electron transport and interfacial charge transfer, which is mainly considered as the rate-determining step for the sluggish electrochemical reaction kinetics of thick electrodes.<sup>[76]</sup>

Polarization can commonly be divided into two types: electrochemical polarization and concentration polarization. For an equilibrium electrode, polarization is the deviation of the potential of this electrode from its equilibrium value as current is passed through the electrode from an external power source.<sup>[78]</sup> Electrochemical polarization and concentration polarization of the anode-electrolyte interface will give rise to the accompanying Zn plating/stripping overpotential. Because of the existence of ultra-thin electric double layers at the interface, although the overpotential is small, polarization will still lead to the enhancement of the interface electric field. Subsequently, many electrons/ions are redistributed at the anode-electrolyte interface, resulting in uneven and uncontrollable Zn deposition, which is not conducive to the realization of dendrite-free anode. The ion concentration discrepancy between the area nearby the electrode surface and the bulk of the electrolyte, which exerts a great impact on dendrite formation. The sluggish ionic transportation in the electrolyte brings the commonly existence of concentration polarization during the deposition of various metal types, including Zn, especially in the organic electrolytes cell systems. As a matter of fact, optimizing concentration electrolyte is often used to deal with this situation, i.e. increasing ionic conductivity. It is worth noting that the weak concentration polarization in this electrolyte system is due to the generally higher ionic conductivity in the aqueous electrolyte than that in the organic electrolyte.

### 2.1.3. Zn<sup>2+</sup> transportation

In fact, Zn<sup>2+</sup> transportation exerts a significant effect on Zn deposition process. The ion transport flux ( $J$ ) of can be written as:

$$J = -\frac{zecD}{kT} \frac{dV}{dx} - D \left[ \frac{dc}{dx} \right] + cV_x \quad (2)$$

where  $z$ ,  $e$ ,  $c$ ,  $D$ ,  $V_x$ ,  $k$ ,  $T$ ,  $V$ , and  $x$  represent the charge number, the unit charge, the ion concentration, the coefficient of diffusion, the convective velocity, the Boltzmann constant, the

thermodynamic temperature, the electric potential, and the distance to the cathode, respectively. The quicker the transfer flux of  $Zn^{2+}$ , the smaller the polarization produced. Therefore, regulating electrolyte concentration and accelerating convection by stirring have been employed to alleviate dendrite formation.<sup>[1]</sup>

#### 2.1.4. Electric field

Lattice defects and residual stress are important reasons for dendrite formation. Taking Zn (002) crystal plane as an example, it is found that the lattice gap caused by defects is an important reason for the interfacial heterogeneous Zn deposition. The Zn deposition activity in the lattice expansion area is higher than that in the compressed area, which will cause the irregular growth of Zn in the local area. Comparing the Gibbs free energy of crystal cell under different strain, it is concluded that Zn crystal is the most stable in the stress-free state. Therefore, Zn is most likely to grow into a stress-free state. The non-uniform electric field at the interface induced by lattice defects greatly affects the behavior of Zn deposition.<sup>[79]</sup>

Admittedly, the nucleation process is also influenced by the interface electric field between anode and electrolyte. Meanwhile, the relatively balanced electric field at the interface can be influenced by random Zn distribution at the nucleation process.<sup>[17]</sup> According to Gauss law, charges are prone to gather near the small tip with large buckling. Therefore, the local electric field is uneven because of the uneven distribution of surface charges. When  $Zn^{2+}$  diffuses near the substrate surface,  $Zn^{2+}$  will be driven to the tip and plated locally. The subsequent deposition also follows the similar rule, and the whole Zn deposition morphology is inclined to be dendritic.<sup>[80]</sup>

#### 2.2. Side reaction

Like mentioned above, the electrochemical HER can evolve hydrogen and produce  $OH^-$  that together with other electrolyte species can further react with Zn anode in thermodynamical and then yield by-products covering on Zn anode surface. Accordingly, the following mechanism analysis of the side reaction (next paragraph) focuses on the HER and the second side reaction, *i.e.*, corrosion reaction.

Zn stripping/electroplating is primarily worked in concert with electrolyte composition and environmental conditions. Understanding the mechanism of hydrogen evolution in different PH electrolytes is conducive to inhibit hydrogen evolution on Zn anode.<sup>[81]</sup>

##### In mildly acid/neutral electrolyte:



$$\varphi_{H^+} = \rho_{H^+}^\theta - \frac{RT}{2F} \ln \frac{1}{\gamma_{H^+}^2 C_{H^+}^2} = -0.24 \text{ V (PH = 4)} \quad (3)$$



##### In alkaline electrolyte:

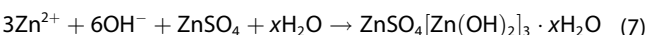


$$\varphi_{H^+} = \rho_{H^+}^\theta - \frac{RT}{2F} \ln (\gamma_{OH^-}^2 C_{OH^-}^2) = -0.83 \text{ V (PH = 14)} \quad (5)$$



where  $R$ ,  $F$ ,  $\rho_{H^+}^\theta$ ,  $\gamma_{H^+}$ ,  $C_{H^+}$  and represent the thermodynamic constant ( $8.31 \text{ J mol}^{-1} \text{ K}^{-1}$ ), temperature, Faraday constant ( $95600 \text{ C/mol}$ ), the standard electrode potential of  $H^+/H_2$  (0 V vs.  $H^+/H_2$ ), activity coefficient for  $H^+$ , and  $H^+$  concentration, respectively. Formulas (4) and (6) show chemical reactions occurring in mildly acidic/neutral and basic electrolytes. Formula (3) and Formula (5) are the electrode reactions on Zn anode under alkaline environment and acidic environment respectively.<sup>[82]</sup> Notably, hydrogen evolution in alkaline electrolytes is even more rampant owing to the large amount of  $OH^-$  involved in the electrochemical reaction.

$Zn(OH)_2$  will be precipitated under ideal thermodynamic conditions when the pH value of electrolyte reaches 5.85. In mildly acidic electrolyte, it is possible to achieve rapid electroplating and stripping of  $Zn^{2+}$  on the surface of the Zn electrode compared with alkaline electrolyte.<sup>[83]</sup> However, it is reported that Zn electrode is highly unstable in slightly acidic  $ZnSO_4$  electrolyte because a nonconductive and loose compound layer ( $Zn_4SO_4(OH)_6 \cdot xH_2O$  (ZHS)) could be generated via the Formula (7).<sup>[84]</sup>



Unfortunately, this loose layer cannot effectively block the electrolyte from contacting with the Zn surface, so it cannot terminate the corrosion reactions by passivating the fresh Zn. A series of side reactions are not conducive to Zn plating/stripping. The continuous HER will increase the concentration of  $OH^-$ , and the resultant byproducts generation and accumulation. The hydrogen bubbles produced by the HER will cause the volume expansion of the anode and bring safety risks.

In addition to HER, corrosion is also a main side reaction on the negative side of AZIBs, usually accompanied by the formation of multitudes of insulating by-products, which seriously affects the uniform deposition of zinc, and declines the zinc metal stability.<sup>[85]</sup> Meanwhile, corrosion reactions consume the active components of the anode and lead to uneven Zn anode surfaces, resulting in low CE and low capacity.<sup>[86]</sup> As a popular belief, the Zn corrosion is mainly caused by its spontaneous side-reactions with electrolyte species, including  $H_2O$ ,  $OH^-$ , and  $H^+$ .<sup>[87]</sup> Generally, formulas (4), (6) and (7) are typically corrosion reactions in AZIBs, implying the concomitant character of the corrosion reaction and hydrogen evolution. As described above, the reactions (4), (6) can lead to the increase of local pH on the Zn surface and thus precipitation of passive by-products (Formula (7)) in  $ZnSO_4$  electrolyte. The existence of passivation layer inevitably reduces the utilization rate of zinc. At present, numerous AILs with the

capability to resist the adverse effects of the corrosion and passivation have been fabricated. For example, it is reported that a  $\text{SiO}_2$ -sodium alginate hybrid film coated onto the Zn metal surface, to manipulate the distribution and chemical environment of  $\text{Zn}^{2+}$ ,  $\text{SO}_4^{2-}$  and  $\text{H}_2\text{O}$  in the Helmholtz layer simultaneously.<sup>[88]</sup> In addition, electrolyte regulation and separator modification are also developed to resist corrosion and passivation.

### 2.3. Protection mechanism of AIL

The protection mechanism of AIL are physical isolation barrier, homogenizing the  $\text{Zn}^{2+}$  flux, optimize nucleation barrier, uniform electrical field, regulate the solvation structure of  $\text{Zn}^{2+}$ , which will be analyzed as follows.<sup>[52,89-92]</sup>

#### 2.3.1. Physical isolation barrier

The direct contact between Zn anode and aqueous electrolyte inevitably brings the corrosion reaction between Zn and electrolyte and further leads to irreversible loss of active Zn anodes. In addition, gas accumulation will also cause the deactivation of Zn electrodes in large sections during discharge process.<sup>[93]</sup> Introducing dense AIL on the surface of Zn foil as a physical isolation barrier has been proved to be a promising strategy to effectively passivate the Zn anode. So far, a variety of materials such as polydopamine (PDA),<sup>[94]</sup> 502 glue,<sup>[95]</sup> UIO66<sup>[96]</sup> have been selected to provide isolate function. Meanwhile, hydrophobic protective layer represented by poly-silane can effectively repel  $\text{H}_2\text{O}$  exposure on the Zn/electrolyte interface to enhance Zn anode stability.<sup>[53]</sup> At the same time, the propyl group in the poly-silane layer increases the flexibility to buffer intrinsic strain/stress, and the hydrophobicity to suppress the electrolyte corrosion.

#### 2.3.2. Homogenize the Zn ion flux

Under deep circulation (high current density and high capacity), the serious interface turbulence can usually destroy the stability of  $\text{Zn}^{2+}$  transmission path. In this regard, the flux distribution of  $\text{Zn}^{2+}$  is affected by two factors: (1) the stability and homogeneousness of the  $\text{Zn}^{2+}$  transport path modulated by the constructed modified layer. (2) The intensity of the inevitable interface turbulence caused by the side reactions. Intense interface turbulence would result in the disorder of ion flux and uneven deposition of Zn,<sup>[97]</sup> which highlight the construction of a robust AIL as a Zn ion flux regulator to induce the uniform ion flux distribution and the subsequent uniform Zn deposition. Various materials, such as MXene nanosheets,<sup>[98]</sup> polymer molecules,<sup>[99]</sup> metal-organic framework (MOF)-based materials,<sup>[31,100,101]</sup> layered  $\alpha$ -Zirconium phosphate,<sup>[102]</sup> have been proposed to construct AILs as a  $\text{Zn}^{2+}$  flux regulator to protect Zn anodes. Specifically, Liu et.al designed a type of polymer molecule interface as an ion-redistributor with dense sulfo-

terminated nanochannels.<sup>[99]</sup> Besides, Su et.al proposed a Janus separator by spray printing of conductive  $\text{Ti}_3\text{C}_2\text{T}_x$  MXene nanosheets over one side of commercial glass fiber separator.<sup>[98]</sup> Recently, Yan et.al constructed an versatile ZrP-based AIL with abundant  $\text{Zn}^{2+}$  channels formed in situ in the interlayers of ZrP.<sup>[102]</sup> The unique layer structure and ion exchange properties of ZrP enable the formation of  $\text{Zn}^{2+}$  channels in the interlayers of ZrP, which can redistribute the  $\text{Zn}^{2+}$  ion flux and promote the  $\text{Zn}^{2+}$  transport at Zn anode/electrolyte interface.

#### 2.3.3. Optimize nucleation barrier

Nucleation is the key factor for the long-term cycling stability of AZIBs. As mentioned above, there are mainly two types of viewpoints about nucleation barrier. Some researchers hold an opinion that zinc is more likely to be deposited at favorable sites with low nucleation overpotential. The low nucleation overpotential is conducive to the initial zinc nucleation and accelerate the subsequent zinc deposition. Furthermore, some researchers have opined that high nucleation overpotential is conducive to the formation of more and finer nuclei. Uniform Zn plating will be realized via increasing nucleation density and decreasing nucleation size. From the above views, controlling Zn nucleation barrier shall be an effective approach to inhibit Zn dendrites. For this issue, various materials have been studied to serve as heterogeneous seeds to reduce nucleation barrier during Zn plating/stripping, such as metal Sn<sup>[74]</sup> or Cu,<sup>[103]</sup> nitrogen-doped Zn (N-Zn),<sup>[104]</sup> nitrogen-doped graphene<sup>[105]</sup> et al. For example, Sn possessing high Zn affinity to reduce nucleation barrier can function as nucleation agent to uniformize Zn deposition.<sup>[74]</sup> Li and colleagues designed the Sn film on Zn plate when Zn reacts in  $\text{SnCl}_2$  solution for a longer/shorter time.<sup>[106]</sup> Cu was applied as AIL following the same preparation principle. Wu et.al. prepared N doped carbon through a liquid-phase process and then coated it on Zn foil.<sup>[107]</sup> Such coating layer endows the Zn anode with lower nucleation overpotential and higher resistance to HER. Similarly, nitrogen as free radicals and active groups that are induced on Zn anode surface, which will improve the Zn plating performance.<sup>[104]</sup> Similarly, many researchers has been devoted to elevating the nucleation barrier. For instance, Liu et al in-situ textured Zn electrode by add  $\text{H}_3\text{PO}_4$  texturing agent.<sup>[108]</sup> The nucleation overpotential after the texturing and addition of  $\text{H}_3\text{PO}_4$  increases from 38 mV to 53 mV. Accordingly, amount nucleus with smaller radius is expected at the higher nucleation overpotential. Wang et.al. introduced sericin molecules as electrolyte additives to regulate the overpotential of Zn nucleation and hydrogen evolution, thereby building a stable solid electrolyte interface (SEI) layer on Zn anode. They also considered that the increased nucleation overpotential of SEI passivated -zinc compared with that of untreated zinc facilitates the formation of many finer grain nucleus.<sup>[109]</sup>

### 2.3.4. Uniform electrical field

Due to the original roughness of the commercial Zn foil surface or the uneven distribution of  $Zn^{2+}$  during the initial deposition, the local electric field near the tip will be significantly enhanced. As a result,  $Zn^{2+}$  is preferentially deposited to the tip during the charging process, resulting in a vicious cycle and eventually evolving into dendrites.<sup>[110]</sup> Wu et al. introduced silicon nanoparticles on the surface of Zn anode to change the charge density.<sup>[111]</sup> Subsequently,  $Zn^{2+}$  preferentially combines with the silicon nanoparticles during the deposition process, forming a Si–O–Zn cross-linked structure *in situ*, which greatly reduces the nucleation barrier of Zn ion. Additionally, the BaTiO<sub>3</sub> layer endowing inherent character of the switched polarization can also adjust electric field distribution to eliminate the “tip effect” and realize dendrite-free Zn anode.<sup>[112]</sup>

### 2.3.5. Regulate the solvation structure of Zn ion

In aqueous electrolytes,  $Zn^{2+}$  are usually surrounded by water molecules. The large hydration radius leads to slow  $Zn^{2+}$  transport kinetics. Therefore, a variety of materials have been reported to prevent the solvation of  $Zn^{2+}$  at the electrolyte-electrode interface, and improving the overall electrochemical reaction activity, such as hydrophobic materials, specific channel materials. Hydrophobically dense coating  $ZnF_2$  also has the ability to reduce desolvation activation energy.<sup>[113]</sup> Owing to a limited size window of 2.94 Å, the artificial MOF layer can prevent the migration of large-sized solvated Zn ion complexes ( $[Zn^{2+}(H_2O)_6 \cdot SO_4^{2-}]$  or  $[Zn^{2+}(H_2O)_5 \cdot OSO_3^{2-}]$ ) (4.7 Å).<sup>[55]</sup> When these complexes migrating in the MOF channels, most of the water in the solvated structure can be excluded via steric effects. At present, typical design strategies of regulating solvation structure include employing concentrated electrolytes, MOF modification and electrolyte additives to modify the ion coordination environment and the electrode/electrolyte interface.<sup>[114]</sup>

## 3. Application of AILs

As mentioned above, the uniform Zn deposition and the inhibition of Zn dendrite are beneficial to the cycling stability and high CE of AZIBs. As described in the reaction mechanism, the protection functions of Zn anodes by AILs can be achieved through five pathways (Figure 2): (1) AILs are used as a physical isolation barrier between Zn anode and electrolyte to resist side reactions and residual products; (2) AILs can serve as a uniform zinc ion flux regulator via promoting uniform deposition; (3) AIL is beneficial for reducing the potential barrier of zinc nucleation due to the zinc affinity of the layer; (4) AILs are designed to uniform the electric field at the interface; (5) AILs destroy the solvation structure of  $Zn^{2+}$ , thus improving the  $Zn^{2+}$  transport and electrode reaction kinetics.

Multifarious materials have been adopted to construct composite AILs to protect Zn anode by far. Inorganic coating

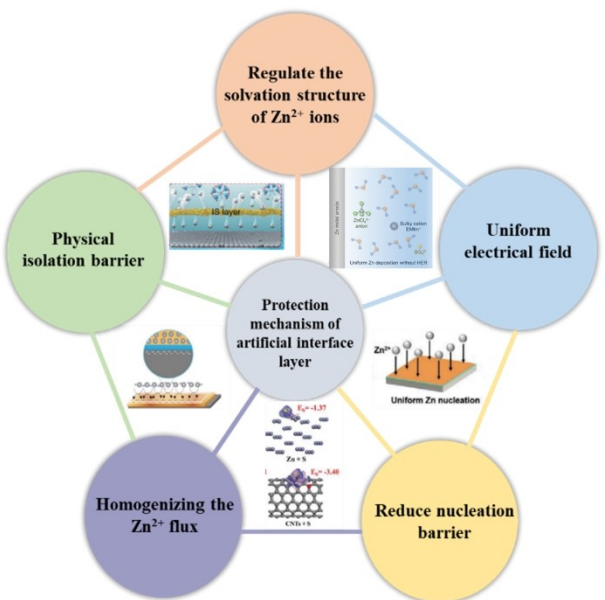


Figure 2. The protection mechanism of AIL. Reproduced from refs. [52, 89–92]. Copyright (2019), with permission from Wiley-VCH. Copyright (2021), with permission from American Chemical Society. Copyright (2022), with permission from Elsevier Ltd. Copyright (2022), with permission from American Chemical Society. Copyright (2021), with permission from Wiley-VCH.

layers are concerned for high mechanical modulus and good surface wettability to reserve electrolyte, while their intrinsically brittle nature and insufficient attraction for Zn ion are difficult to achieve robust  $Zn^{2+}$  flux regulation. Organic component layers with good flexibility can maintain good contact with Zn metal and strong regulation of  $Zn^{2+}$  flux via polar groups, but mechanical strength of some of them cannot support high-capacity and long-term cycles.<sup>[84]</sup> Therefore, the construction of composite layers is more effective in protecting zinc anodes, and organic-inorganic composites are most common. It is undeniable that some inorganic materials also have good flexibility (such as graphene oxide (GO),  $Ti_3C_2T_x$  MXene), and some organic materials also exhibit certain mechanical strength (such as covalent organic framework) due to their crystal structure. In addition, AIL constructed through *in-situ* methods such as adding electrolyte additives can also generate inorganic-inorganic or organic-organic protective layers. In the consideration of the multifunctionality of one modified component, the following discussion is classified by the types of materials instead of specific function of AILs. Accordingly, three categories are divided as follows: organic-inorganic composite AILs, inorganic-inorganic composite AILs, and organic-organic composite AILs.

The specific experimental process that can present an ex-situ or *in-situ* method to construct composite AILs, is taken as the basis of the subcategory. Next, the multifunctionality of the three kinds of composite AILs and their positive effect towards Zn anode will be discussed in detail.

### 3.1. Inorganic-organic composite AILs

#### 3.1.1. Inorganic-organic composite AILs synthesized by ex-situ

The ex-situ preparation of composite AILs method is generally done by putting a pre-synthetic coating through solution casting (blade coating, spin coating, drop coating), sputtering, dip coating,<sup>[51,115]</sup> atomic/molecular layer deposition,<sup>[116,117]</sup> 3D printing<sup>[118,119]</sup> etc. The ex-situ preparation method is equipped with advanced merits. (1) The engineering workflow of the ex-situ method is simple. (2) The method is extremely cost-effective due to the high material utilization rate. (3) The thickness, uniformity, and stability of deposited layer can be controlled precisely by ex-situ method, which leads to high repeatability. These advantages make ex-situ method competitive for large-scale applications. Thereby, most composite inorganic-organic AILs are synthesized by ex-situ method (Table 1).

Composite AILs synthesized by ex-situ typically consists of three parts: inorganic material, organic material, and adhesives (generally refer to polyvinylidene fluoride (PVDF)). Inorganic materials modified by organic compounds can be referred to as hybrid AILs with inorganic hosts. Similarly, organic materials are modified by inorganic substances, which we refer to as hybrid AILs with organic hosts. In addition, adhesives are also widely modified to improve its conductivity and flexibility. Based on the modified materials, organic-inorganic hybrid AILs are divided into three categories: hybrid AILs with inorganic hosts, hybrid AILs with organic hosts, and hybrid AILs with modified PVDF.

##### 3.1.1.1. Hybrid AILs with inorganic hosts

Intercalation type inorganic compounds are typical materials to construct organic-inorganic composite AILs due to their potential intrinsic capability to provide  $Zn^{2+}$  transport channels that can modulate uniform  $Zn^{2+}$  flux and the subsequent Zn deposition.  $Zr(HPO_4)_2 \cdot H_2O$  ( $\alpha$ -ZrP) exhibits a good thermal stability, a low electronic conductivity and a high resistance to acid and alkali, all of these advanced characters demonstrate  $\alpha$ -ZrP can be conducted as an excellent inorganic material for composite protective layer. However, the interlayer spacing of untreated  $\alpha$ -ZrP is far less than the diameter of water and  $Zn^{2+}$ . To solve this problem, Peng et.al successfully produced a layer-structured  $\alpha$ -ZrP nanoplates with an expanded interlayer spacing by the intercalation of n-butylamine (marked as ex-ZrP).<sup>[120]</sup> As showed in Figure 3(A), the thickness of ZrP nanoplate was expanded from 35 nm to 120 nm after the insertion of n-butylamine. Therefore, the intercalation of n-definite amine prominently widens the layer spacing of  $\alpha$ -ZrP and promotes the dissolution and migration of  $Zn^{2+}$ . Furthermore, due to the similar polarity of n-definite amine and NMP/PVDF (auxiliary materials when constructing the AIL), the compatibility between ex-ZrP and NMP/PVDF can be highly improved, thus enhancing the compactness of the composite layer. The intercalated layer successfully facilitated the electrochemical performances of Zn

anode. The symmetrical cell of Zn/ex-ZrP ran more than 3000 cycles at a capacity of  $1\text{ mAh cm}^{-2}$  and a current density of  $6\text{ mA cm}^{-2}$  (Figure 3B). Similarly, the limited interlayer spacing of montmorillonite is not conducive to the rapid transport of  $Zn^{2+}$ . Wang and his collaborators designed hexadecyl trimethyl ammonium bromide (CTAB) as a support to embed in the interlayer of layered montmorillonite, and enlarge the interlayer spacing of raw montmorillonite (RMMT) from 1.50 nm to 1.93 nm, as shown in Figure 3(C).<sup>[121]</sup> Interestingly, the modified montmorillonite can not only be used as the protective layer of Zn anode to inhibit Zn dendrite, but also as the protective layer of manganese dioxide to prevent its dissolution.

Aside from intercalation type composite AIL, a Janus separator AIL based on a Zn-ion conductive metal organic framework (MOF) as an inner layer and reduced graphene oxide (RGO) as an outer layer was reported to regulate uniform  $Zn^{2+}$  flux and electron conduction (Figure 3D).<sup>[122]</sup> X-ray diffraction (XRD) pattern shows that the synthetic MOF is pure MOF808 (Figure 3E). Anionic MOF provides a  $Zn^{2+}$ -rich layer near the surface of Zn anode through electrostatic interaction and regulates uniform  $Zn^{2+}$  flux with the inner well-defined anionic sub-nano tunnels. Meanwhile, the RGO serves as a stable electro-conductive layer on top surface of Zn anode, which not only reduces  $Zn^{2+}/Zn$  redox barrier on current collector but also increases the reversibility of Zn anode by digesting "dead Zn" during cycling. As depicted in Figure 3(F), the anode shows both enhanced self-corrosion potential (from 0.016 to 0.032 V) and lowered self-corrosion current (from 2.63 to 0.71  $\text{mA cm}^{-2}$ ) under the guidance of MOF/RGO protective layers, indicating a higher electrochemical stability against corrosion in anode-electrolyte interface. The usage of Zn anode with MOF/RGO functional layer prominently enhanced the CE, cycling stability and magnification electrochemical performance of Zn anode, and obtained high-performance Zn// $MnO_2$  full battery. It exhibits stable cycling performance (nearly 100% capacity retention) with a reversible capacity of  $135\text{ mAh g}^{-1}$  over 2000 cycles, far beyond that of the unmodified Zn// $MnO_2$  full battery ( $25\text{ mAh g}^{-1}$  over 1000 cycles).

In the process of Zn plating/stripping, the chaotic distribution of  $Zn^{2+}$  has an influence on the uniformity of the interfacial electric field. The interfacial electric field plays a key role in the uniform growth of Zn. Therefore, regulating the balance of interfacial electric field can effectively guide the uniform nucleation of Zn and inhibit Zn dendrites.<sup>[69,123,124]</sup> Some materials endowed with special high electric constant can be employed to modulate the ion distribution under an external electric field. Amorphous silicon nitride ( $Si_3N_4$ ) nanoparticles with abundant dangling bonds ( $N_3Si$ ,  $Si_2N$ , etc.) is the typical example to realize this function.<sup>[125]</sup> Under the control of the applied electric field, the dipole moment can be arranged in a specific direction, which can guide the distribution/migration of  $Zn^{2+}$  in the electrolyte (Figure 4A). However,  $Si_3N_4$  as inorganic material usually possess high hardness, lacking in the ability to change self-volume accompany with the swell of battery cycle. Polyacrylonitrile (PAN) with superior elasticity and mechanical properties can act as a barrier layer to isolate  $H_2O/O_2$ . Therefore, AIL with the synergistic effect of  $Si_3N_4$  and PAN can effectively

Composite AILs	Protection mechanism	Fabricating method	Hysteresis voltage	Cyclic lifespan	Ref.
CTAB/ZnOMMT <sup>[a]</sup>	Homogenize the Zn ion flux; Optimize nucleation barrier	Blade coating	47 mV	1100 h at 1.0 mAcm <sup>-2</sup> and 1.0 mAcm <sup>-2</sup>	[121]
Ex-ZRP/PVDF <sup>[b]</sup> (~120 nm)	Regulate Zn <sup>2+</sup> solvation structure; Optimize nucleation barrier	Blade coating	164 mV	~3000 cycles at 6 mAcm <sup>-2</sup> and 1 mAcm <sup>-2</sup>	[120]
ZIF-8/GO (4 μm)	Homogenize the Zn <sup>2+</sup> flux; Regulate Zn <sup>2+</sup> solvation structure	Blade coating	108 mV	2180 h at 0.5 mAcm <sup>-2</sup> and 0.5 mAcm <sup>-2</sup>	[138]
MOF/RGO	Homogenize the Zn <sup>2+</sup> flux; Uniform electrical field	Blade coating	75 mV	over 500 h at 0.5 mAcm <sup>-2</sup>	[122]
Si <sub>3</sub> N <sub>x</sub> /PAN <sup>[c]</sup> (10 μm)	Homogenize the Zn <sup>2+</sup> flux; Physical isolation barrier	Dip coating	60 mV	800 h at 1.0 mAcm <sup>-2</sup> and 1.0 mAcm <sup>-2</sup>	[125]
ZrO <sub>2</sub> /cellulose	Homogenize the Zn <sup>2+</sup> flux; Optimize nucleation barrier;	Solution casting	84 mV	over 1000 h 5 mAcm <sup>-2</sup> and 2.5 mAcm <sup>-2</sup>	[126]
PVA@SR <sup>[d]</sup> /ZnMoO <sub>4</sub>	Uniform electrical field	Blade coating	≈ 80 mV	2000 h at 2 mAcm <sup>-2</sup> and 2 mAcm <sup>-2</sup>	[127]
MXene/mPPy <sup>[f]</sup>	Homogenize the Zn <sup>2+</sup> flux; Regulate Zn <sup>2+</sup> solvation structure. Physical isolation barrier;	Blade coating	≈ 80 mV	over 900 h at 1 mAcm <sup>-2</sup> and 1 mAcm <sup>-2</sup>	[136]
MXene/mPPy <sup>[f]</sup>	Uniform electrical field	Spray coating	29 mV	1000 h at 1 mAcm <sup>-2</sup> and 1 mAcm <sup>-2</sup>	[137]
PVDF/SBA15 <sup>[g]</sup>	Homogenize the Zn <sup>2+</sup> flux; Uniform electrical field	Spin coating	≈ 120 mV	over 1650 h at 3 mAcm <sup>-2</sup> and 0.6 mAcm <sup>-2</sup>	[139]
Zr-MOF/PVDF-HFP <sup>[h]</sup>	Homogenize the Zn <sup>2+</sup> flux; Physical isolation barrier	Blade coating	≈ 110 mV	over 240 h at 10 mAcm <sup>-2</sup>	[146]
UIO-66 MOFs/SPEEK <sup>[i]</sup>	Homogenize the Zn <sup>2+</sup> flux; Physical isolation barrier	Solution casting	—	over 700 h at 5 mAcm <sup>-2</sup> and 5 mAcm <sup>-2</sup>	[147]
Zn-MMT <sup>[j]</sup> /PVDF-HFP	Uniform electrical field; Physical isolation barrier	Blade coating	—	over 3000 h at 1 mAcm <sup>-2</sup> and 1 mAcm <sup>-2</sup>	[141]
PDMS/TiO <sub>2-x</sub> <sup>[k]</sup>	Physical isolation barrier;	Spin coating	80 mV	900 h at 1 mAcm <sup>-2</sup> and 1 mAcm <sup>-2</sup>	[145]
	Optimize nucleation barrier				

[a] CTAB refers to hexadecyl trimethyl ammonium bromide. Zn-OMMT refers to pillared organic montmorillonite with ZnSO<sub>4</sub>/MnSO<sub>4</sub> solution. [b] Ex-ZRP refers to a layer-structured α-ZnP (Zr(HPO<sub>4</sub>)<sub>2</sub>·H<sub>2</sub>O) nanoplates with an expanded interlayer spacing by the intercalation of n-butylamine. PVDF is the abbreviation of Poly vinylidene fluoride auxiliary materials. [c] PAN is the abbreviation of polyacrylonitrile. [d] PVA is a polymer called polyvinyl alcohol. SR: SO<sub>4</sub><sup>2-</sup> receptor. [e] PAM is a polymer called polyacrylic amide. PVDF-HFP is poly vinylidene fluoride-hexafluoropropylene. [f] mPPy is a polymer called polypyrrole. [g] SBA15 is an inorganic Santa Barbara Amorphous-15. [h] PVDF-HFP is the abbreviation of the poly vinylidene fluoride-hexafluoropropylene. [i] SPEEK is the abbreviation of the sulfonated poly (ether ketone). [j] Zn-MMT refers to Zn-montmorillonite. [k] PDMS is a highly self-adaptable poly(dimethyl)siloxane].

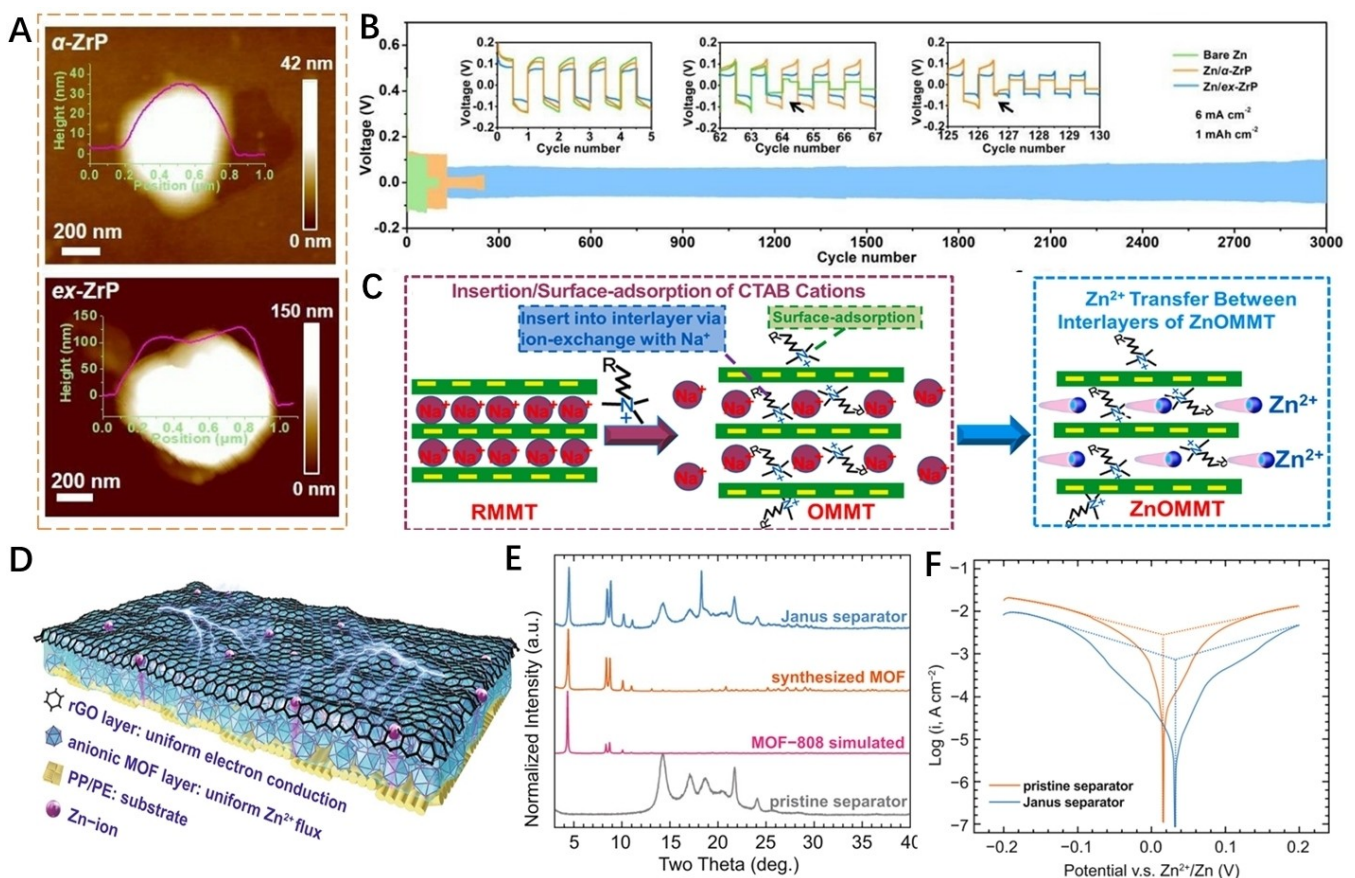


**Figure 3.** A) AFM images with height profiles. B) Voltage profiles of the symmetrical cells at 6 mA cm<sup>-2</sup> current densities and 1 mAh cm<sup>-2</sup> plating/stripping capacity in ZnSO<sub>4</sub> electrolyte. Ex-ZrP refers to a layer-structured  $\alpha$ -ZrP ( $Zr(HPO_4)_2 \cdot H_2O$ ) nanoplates with an expanded interlayer spacing by the intercalation of n-butylamine. Reproduced from ref. [120]. Copyright (2022), with permission from The Royal Society of Chemistry. C) Schematic of insertion/surface-adsorption of CTAB cations for organic montmorillonite (OMMT) and Zn ion transfer between interlayers of Zn-OMMT. CTAB is the abbreviation of hexadecyl trimethyl ammonium bromide. Zn-OMMT refers to pillared organic montmorillonite with ZnSO<sub>4</sub>/MnSO<sub>4</sub> solution. Reproduced from ref. [121]. Copyright (2022), with permission from Elsevier Ltd. D) Schematic illustration for the MOF/RGO composite AIL. MOF = Metal-organic frame structure. RGO = reduced graphene oxide. E) XRD patterns of the simulated MOF-808, synthesized MOF, the pristine separator and Janus separator. F) Linear polarization curves of the Zn/Zn symmetric cells with Janus and pristine separators at a scan speed of 1 mV s<sup>-1</sup> in 2 M ZnSO<sub>4</sub> aqueous electrolyte. Reproduced from ref. [122] Copyright (2021), with permission from Springer Nature.

suppress the anodic corrosion and boost the Zn<sup>2+</sup> kinetics and electrical stability of Zn anodes. As shown in Figure 4(B), Zn<sup>2+</sup> tends to accumulate at the sites with a high curvature, which could evolve into dendrites on blank Zn foil. On the contrast, the Zn<sup>2+</sup> migration on the Zn foil with the composite AIL (denoted with PSN in Figure 4C) experiences a brief 2D unstable diffusion then proceeds into a stable 3D diffusion process. Similarly, due to high electric constant of ZrO<sub>2</sub>, the favorable Maxwell-Wagner polarization generated. Similarly, due to high electric constant of ZrO<sub>2</sub>, the favorable Maxwell-Wagner polarization generated from ZrO<sub>2</sub> under external electric field can provide a homogeneous-distributed electric field around the interface to regulate Zn deposition reduce the nucleation overpotential, and inhibit the Zn metal corrosion. and. To remedy the flexibility of ZrO<sub>2</sub>, high ionic conductive, superior flexibility and low-cost cellulose nanofibers were prepared to fabricate a composite AIL with ZrO<sub>2</sub>. Ultimately, the composite AIL enables the highly reversible Zn<sup>2+</sup> plating/stripping behaviors (Figure 4D).<sup>[126]</sup>

In view of the fact that a single inorganic-components AIL may easily fall off or break from the anode surface, Chen et.al constructed a multifunctional composite AIL, *i.e.*, polyvinyl alcohol (PVA) @ SR/ZnMoO<sub>4</sub> (SR: SO<sub>4</sub><sup>2-</sup> receptor)/PVA to modulate the irregular Zn deposition.<sup>[127]</sup> The outer gel layer PVA@SR can trap SO<sub>4</sub><sup>2-</sup>, which accelerates the migration and diffusion of Zn<sup>2+</sup> cations. ZnMoO<sub>4</sub> can improve Zn<sup>2+</sup> conduction retardation by establishing rapid Zn<sup>2+</sup> migration channels with PVA gels. As demonstrated in Figure 4(E), the ion migrating coefficient of the composite ZnMoO<sub>4</sub>/PVA@SR coating is prominently faster than that of the single coatings. Therefore, coordination between PVA@SR and ZnMoO<sub>4</sub> can effectively inhibit dendrite growth and HER to stabilize the Zn anode, especially under high current and capacity. Both the symmetric cell as well as the full cell exhibit relatively stable 3D diffusion after brief 2D diffusion, resulting in dense nucleation sites and the suppressed side reaction (Figure 4F,G).

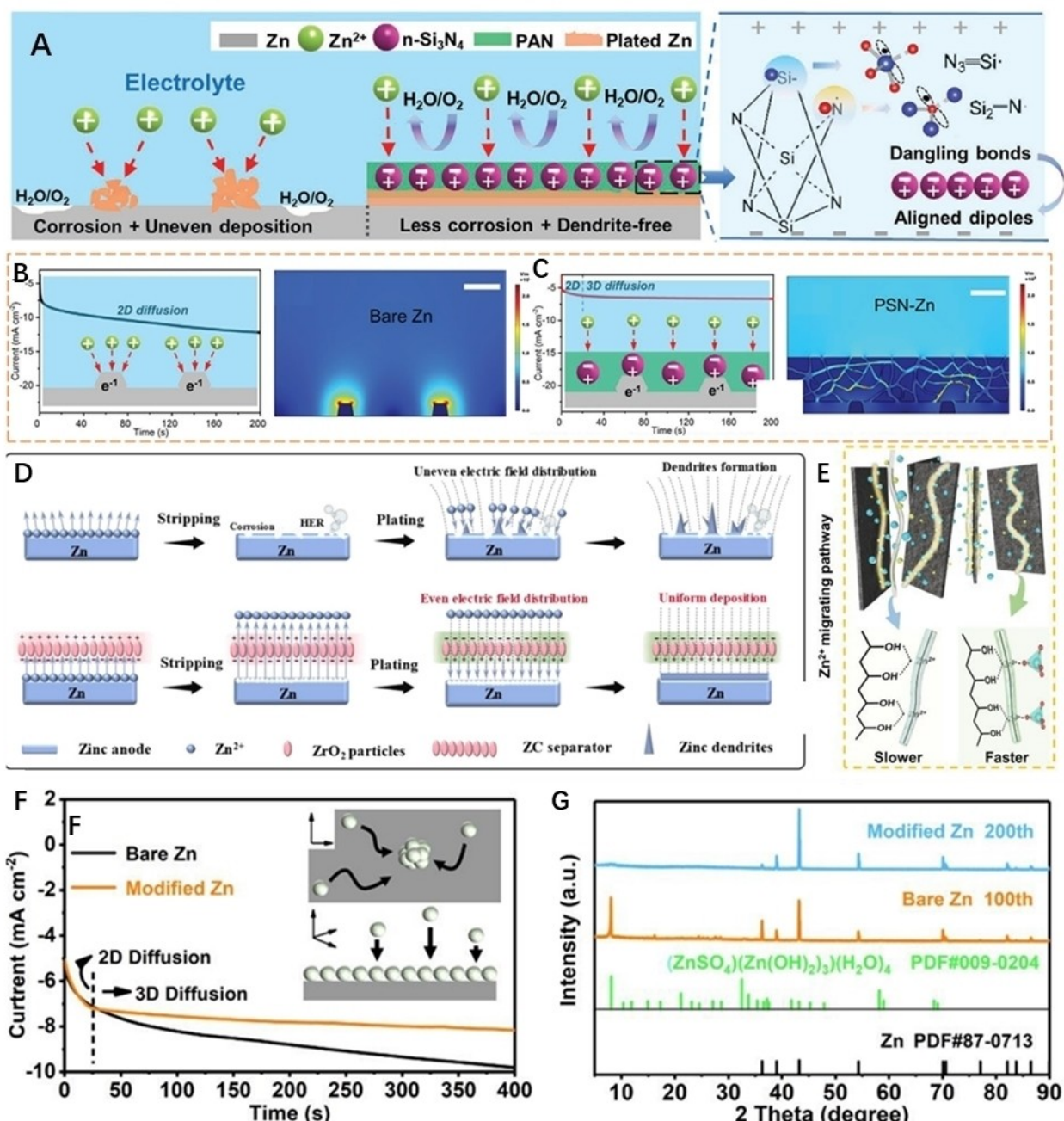


**Figure 4.** A) Schematic illustration of Zn plating/stripping on bare Zn (left panel) and Zn with PSN coating (middle panel). The right panel shows that the amorphous  $\text{Si}_3\text{N}_4$  nanoparticles exhibit novel dielectric behaviour. PSN = polyacrylonitrile (PAN) matrix decorated with amorphous  $\text{Si}_3\text{N}_4$  nanoparticles. B) Chronoamperometry (CA) at  $-200 \text{ mV}$  of overpotential and the corresponding illustration of the  $\text{Zn}^{2+}$  diffusion and reduction processes (inset) for bare Zn. (Left panel). The right panel shows electric field distribution for bare Zn. C) Chronoamperometry at  $-200 \text{ mV}$  of overpotential and the corresponding illustration of the  $\text{Zn}^{2+}$  diffusion and reduction processes (inset) for PSN-Zn electrodes. (Left panel). The right panel shows electric field distribution for PSN-Zn electrodes. Reproduced from ref. [125] Copyright (2021), with permission from Wiley-VCH. D) Schematic illustration of possible migration process of  $\text{Zn}^{2+}$  when passing through the cellulose and ZC separators. Reproduced from ref. [126] Copyright (2022), with permission from Elsevier Ltd. E) Schematics of Zn ion migration in the migrating pathway at the  $\text{ZnMoO}_4/\text{PVA}$  interface in the hybrid inner layer. F) Chronoamperometry plots of bare Zn and modified Zn by  $\text{ZnMoO}_4/\text{PVA}$ . PVA = polyvinyl alcohol. G) XRD patterns after cycling (removing the modification layer of Modified Zn anode). Reproduced from ref. [127]. Copyright (2023), with permission from The Royal Society of Chemistry.

### 3.1.1.2. Hybrid AILs with organic hosts

Diversified physicochemical properties make organic polymer a promising candidate to tackle the mentioned issues of the Zn anode.<sup>[128–130]</sup> On the organic polymer layer, there are various

polar groups that can regulate the uniform flux of  $\text{Zn}^{2+}$ . Simultaneously good flexibility enables it to fully contact with Zn metal. But some organic polymer's mechanical strength is usually poor, fail to resist the Zn dendrite penetration during long battery cycle, especially at high capacity. Therefore, the

organic polymers are generally combined with inorganic material to afford the sufficient mechanical strength and restrain side reactions and Zn dendrite, including 2D materials MXene, porous materials (UIO-66 MOFs, SBA15, ZIF-8 decorated GO (ZGL)), layered mineral Zn-based montmorillonite, defective material  $\text{TiO}_{2-x}$ .

The organic polymers coordinated with MXene have been proved to be suitable for constructing composite AILs.  $\text{Ti}_3\text{C}_2\text{T}_x$  MXene is a typical 2D layered material consist of two C atomic and three Ti atomic layers in  $\text{TiCTiCTi}$  arrangement.<sup>[131]</sup> In this structure, two dense Ti atom layers are exposed on the surface, showing a hexagonal compact packed crystal structure similar to that of electrodeposited Zn.<sup>[132]</sup> A lattice mismatch between Ti-terminated surface of (0002) plane of  $\text{Ti}_3\text{C}_2\text{T}_x$  and (0002) plane of Zn deposits is only 10% (Figure 5A). Such a low lattice mismatch can induce Zn to continuously nucleate at the crystal surface and the formation of a oriented deposition along the Zn(002) plane, which does not lead to uncontrolled dendrite growth.<sup>[133]</sup> Meanwhile,  $\text{Ti}_3\text{C}_2\text{T}_x$  MXene has a high specific surface area and a high conductivity similar to graphene.<sup>[134-135]</sup> Consequently, MXene has been reported to synthesize inorganic-organic AIL with different polymers including polypyrrole (mPPy), polyacrylamide (PAM). In fact, the introduction of MXene nano-filler is also expected to improve the dielectric constant of the polymer to form a local polarized electric field and promote the dissociation of Zn salt. Besides, the high thermal conductivity of MXene enhances the thermal diffusion of  $\text{Zn}^{2+}$  at the electrode-electrolyte interface, especially under the condition of rapid charging and discharging.<sup>[59]</sup> For instance, Wang and his cooperators report a one-step coating strategy assisted by MXene to fabricate a MXene-PAM AIL composites on Zn foil (Figure 5B).<sup>[136]</sup> PAM was used as coating layers to enhance the life span of ZIBs by shielding physically to suppress the side reactions and guiding transport kinetics of  $\text{Zn}^{2+}$  while MXene nanosheets served as nanofillers to further enhance the mechanical strength and ionic conductivity of the polymer coating. As a result, under MXene-PAM AIL protection, symmetric Zn//Zn cells realized a steady cycling performance over 1900 h at a current density of  $0.2 \text{ mA cm}^{-2}$ , (Figure 5C). Additionally, MXene based polypyrrole (MXene-mPPy) layers with high charge capabilities on Zn foil has also been developed for dendrite-free Zn metal anode as well as (Figure 5D-F).<sup>[137]</sup>

Organic polymers can also be combined with porous materials to construct composite AILs. Gan and his cooperators fabricated a polymeric PVDF layer reinforced by a ZIF-8 decorated graphene oxide (GO) (composite layer was defined as ZGL) to modulate the deposition behaviors of  $\text{Zn}^{2+}$ .<sup>[138]</sup> According to density functional theory (DFT), the binding energy of Zn atoms on ZIF-8 is much higher than that on bare Zn (Figure 5G). It means that ZIF-8 possess a stronger affinity to  $\text{Zn}^{2+}$  at the electrode-electrolyte interface than bare Zn surface. Thus, the obtained ZGL can homogenize the  $\text{Zn}^{2+}$  flux distribution, notably reduce the desolvation active energy, and promote a smooth Zn deposition. The corresponding Zn||Zn symmetric cell cycled more than 2400 h with a cumulative capacity of  $12000 \text{ mAh cm}^{-2}$  at  $10 \text{ mA cm}^{-2}$  (Figure 5H). Re-

cently, hydrophobic organic-inorganic PVDF-SBA15 AIL was constructed on the Zn anode.<sup>[139]</sup> SBA15 with uniformly distributed of porous structure can provide homogeneous diffusion channels for  $\text{Zn}^{2+}$  transportation, which is conducive to realize uniform nucleation and growth of Zn (Figure 6A). PVDF with excellent hydrophobic property enable modified layer to increase the water resistance of Zn anode surface. Consequently, the modified Zn anode exhibited a higher dynamic contact angles towards electrolyte than that of bare Zn (Figure 6B) and thus inhibited the potential side reactions between free water molecules and zinc anode. The Zn|| $\text{V}_2\text{O}_5$  full cell lifespan was remarkably promoted by such a PVDF-SBA15 composite AIL (nearly 82.14% capacity retention after 1000 cycles at  $1 \text{ Ag}^{-1}$ ).

In addition to combining with MXene and porous materials to form a protective layer, the organic polymer coating can also combine with layered mineral montmorillonite to form a stable Zn anode composite AIL. Montmorillonite is a three-layer lamellar Clay mineral composed of  $\text{Al}_2\text{O}_3$  octahedron in the middle and  $\text{SiO}_2$  tetrahedron in the top and bottom (Figure 6C). The tetrahedral and octahedral sheets in smectite layers are negatively charged, compensated by hydrated cations located in the interlayer space (Including  $\text{Na}^+$ ,  $\text{K}^+$ ,  $\text{Li}^+$ ,  $\text{Ca}^{2+}$ ,  $\text{Mg}^{2+}$ ). The positively charged layered edges, negatively charged interfaces and interlayers conjointly offer highways for ion exchange and transport of cations (e.g.  $\text{Zn}^{2+}$ ,  $\text{Li}^+$ ,  $\text{Ca}^{2+}$ , and  $\text{Na}^+$ ).<sup>[121,140]</sup> Therefore, the Zn- montmorillonite (Zn-MMT) can be produced by ion exchange and adopted as an inorganic filler to optimize the Zn ion transfer kinetics, further improving the protective efficacy of polymer composite coating. Based on the poly vinylidene fluoride-hexafluoropropylene (PVDF-HFP), co-doped with poly(ethylene oxide) (PEO) and Zn-MMT, Liu et al. fabricated a biomimetic polymer-clay nanocomposite coating for dendrite-free Zn metal anode.<sup>[141]</sup> As shown in Figure 6(D), due to the excellent mechanical properties of Zn-montmorillonite, the mechanical strength of the composite layer can be significantly improved with just a little addition amount because H-F and H-O hydrogen bonds are formed between PEO and PVDF and Zn-montmorillonite, respectively, benefitting from the fabricated porous polymer network. The AIL can restrict the contact between Zn and electrolyte, accelerate  $\text{Zn}^{2+}$  conduction and uniformize Zn growth.

Organic polymers can also be combined with defective materials  $\text{TiO}_{2-x}$ . Titanium dioxide ( $\text{TiO}_2$ ) has excellent electrical properties due to its high dielectric constant. Therefore, its ability to conduct Zn ions is outstanding.<sup>[142]</sup> Unfortunately, owing to the tight encapsulation of Ti atoms and oxygen atoms in  $\text{TiO}_2$ , the insertion of Zn ion could trigger volume expansion, resulting in poor long-term stability.<sup>[143]</sup> Elegant structure design and nanoengineering are suggested to solve the volume expansion.<sup>[144]</sup> Guo et.al proposed a highly dynamic and self-adaptable poly(dimethyl-siloxane) (PDMS)/ $\text{TiO}_{2-x}$  composite AIL (Figure 6E).<sup>[145]</sup> The rapid and uniform transfer of  $\text{Zn}^{2+}$  was achieved by the introduction of oxygen vacancy-rich  $\text{TiO}_{2-x}$ . DFT calculation showed the vacancy-containing  $\text{TiO}_{2-x}$  had repulsive effect toward  $\text{Zn}^{2+}$  and thus prompted the diffusion of  $\text{Zn}^{2+}$  (Figure 6F). The high dynamic adaptability of PDMS

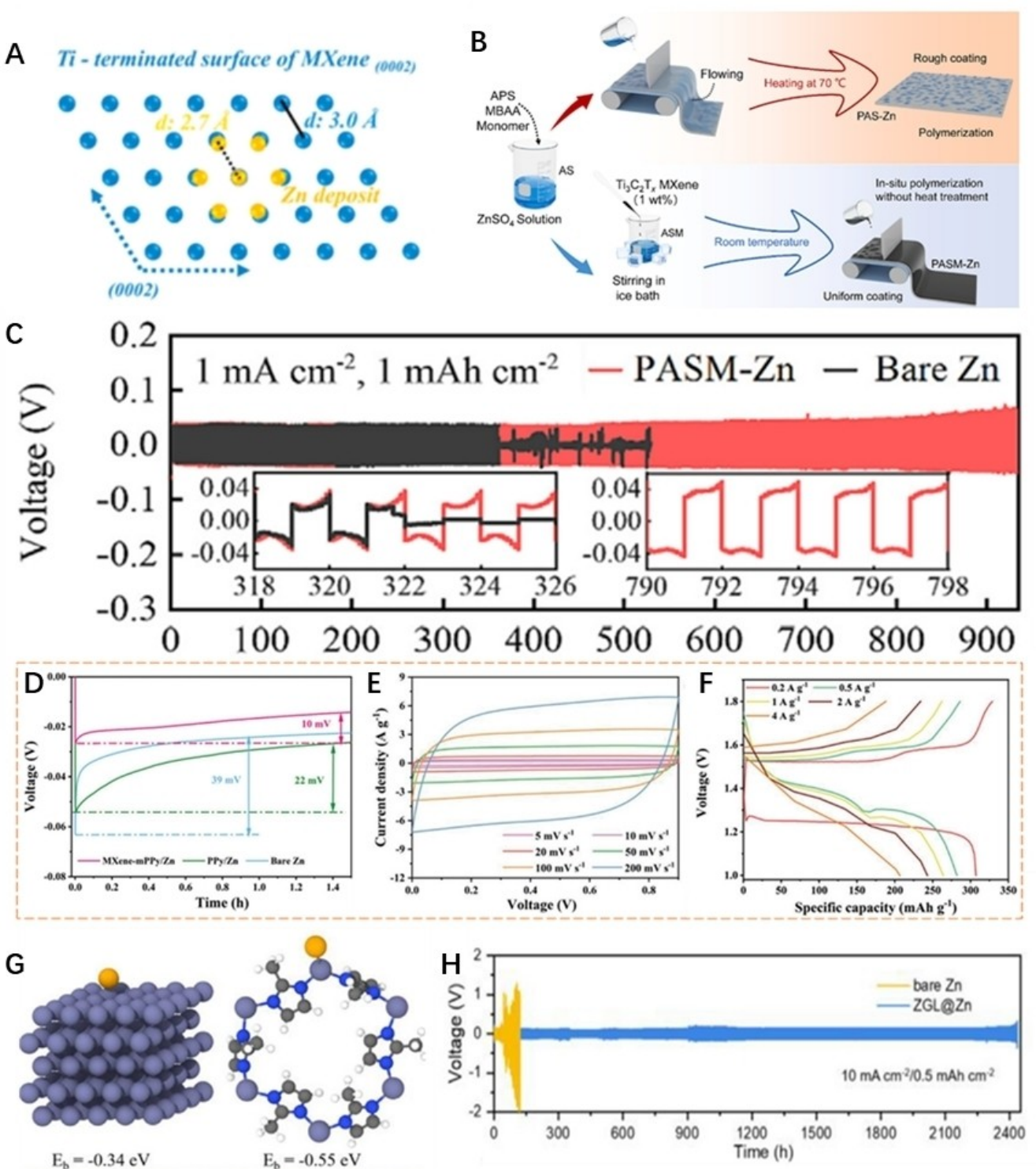


**Figure 5.** A) The atomic arrangements of Ti terminated surface of  $\text{Ti}_3\text{C}_2\text{T}_x$  MXene (0002) and Zn deposits (0002). Reproduced from ref. [132]. Copyright (2021), with permission from American Chemical Society. B) Schematic diagram of one-step preparation of polymer coatings from aqueous monomer solutions with the assistance of  $\text{Ti}_3\text{C}_2\text{T}_x$  MXene. When combined with MXene, it can be polymerized at room temperature, and a uniform, continuous, and adhesive polymer film can be formed using the doctor-blade coating technology. APS refers to the initiator ammonium persulfate. MBAA refers to the crosslinking agent N,N'-methylenebisacrylamide. Monomer refers to 2-Acrylamido-2-methylpropanesulfonic acid (AMPS) powder and acrylic acid (AA). ASM = AA-AMPS-MXene. PAS-Zn refers to P(AA-co-AMPS)-Mxene coated zinc. C) Cyclic performance of Zn//Zn symmetrical batteries at  $1 \text{ mA cm}^{-2}$  with areal capacities of  $1 \text{ mAh cm}^{-2}$  in the  $2 \text{ M ZnSO}_4$  electrolytes. Reproduced from ref. [136]. Copyright (2022), with permission from Elsevier Ltd. D) Nucleation overpotentials of Zn plating on bare Zn, PPy/Zn, and MXene-mPPy/Zn, showing the lowest overpotential of  $10 \text{ mV}$  for MXene-mPPy/Zn in  $2 \text{ M ZnSO}_4$  electrolyte. mPPy is a polymer called polypyrrole. E) CV curves of symmetric capacitors with MXene-mPPy/Zn electrodes, showing a large and stable specific capacitance for MXene-mPPy/Zn electrode. F) Charge/discharge voltage profiles of  $\text{MnO}_2/\text{MXene-mPPy/Zn}$  full cells at various current densities. Reproduced from ref. [137]. Copyright (2022), with permission from Wiley-VCH. G) Calculated binding energy of a Zn atom adsorbed on Zn (001) (left) and ZIF-8 (right). H) Long-term cycling performance of the bare Zn and ZGL@Zn symmetric cells at  $10 \text{ mA cm}^{-2}$  current densities and  $5 \text{ mAh cm}^{-2}$  capacities in  $2 \text{ M ZnSO}_4$  electrolyte. ZGL@Zn refers to Zn anode coated by a ZIF-8 decorated GO (ZGL). Reproduced from ref. [138]. Copyright (2022), with permission from Elsevier Ltd.

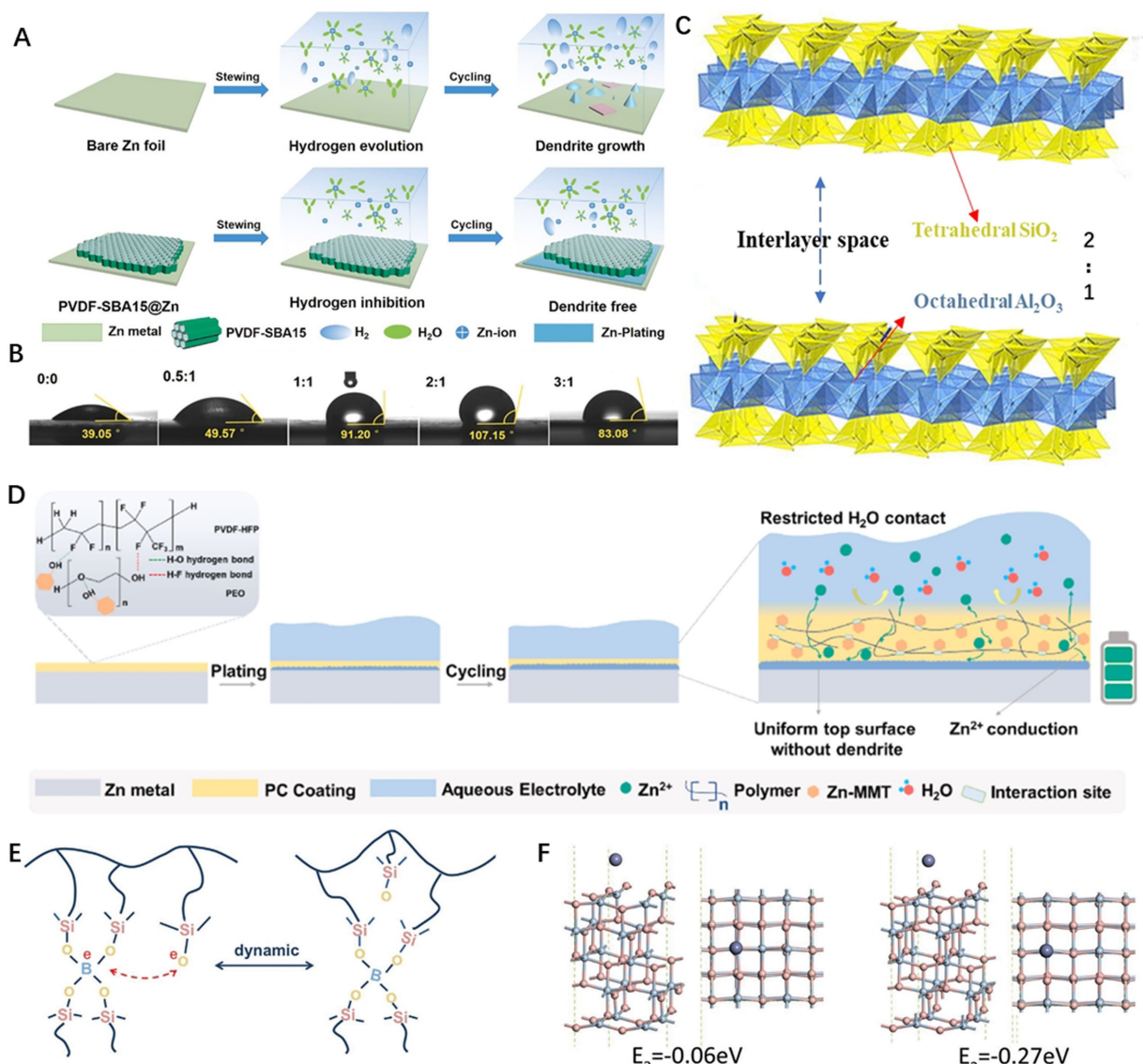


**Figure 6.** A) The side reactions of bare Zn and PVDF-SBA15@Zn anodes in the  $\text{ZnSO}_4$  electrolyte. B) The dynamic contact angles of deionized water on the surface bare Zn and PVDF-SBA15@Zn (different ratio of PVDF and SBA15). PVDF is the abbreviation of Poly vinylidene fluoride auxiliary materials. SBA15 refers to an inorganic Santa Barbara Amorphous-15. Reproduced from ref. [139]. Copyright (2022), with permission from Elsevier Ltd. C) Structural diagram of montmorillonite. Reproduced from ref. [140]. Copyright (2022), with permission from Elsevier Ltd. D) The PC can suppress dendrite growth, passivation, corrosion, and  $\text{H}_2$  evolution, facilitating fast  $\text{Zn}^{2+}$  diffusion and uniform electrochemical deposition. PC = polymer-clay composite coating, MMT = Montmorillonite. Reproduced from ref. [141]. Copyright (2023), with permission from Elsevier Ltd. E) The dynamic micro-crosslinking of the B–O bonds. F) Theoretical simulation models and surface adsorption energy of Zn with  $\text{TiO}_2$  (Left) and  $\text{TiO}_{2-x}$  (Right). Reproduced from ref. [145]. Copyright (2022), with permission from Wiley-VCH.

host can further alleviate the volume changes attributing to the micro-crosslinking of the B–O bonds. Impressively, the protected anode was featured by long cyclic stability for more than 300 h at a current density of  $10 \text{ mA cm}^{-2}$ , displaying excellent potential as an anode for AZIBs.

### 3.1.1.3. Hybrid AILs with modified PVDF

Besides, the most widely used adhesive is PVDF at present, which has good electrochemical stability, and high bonding strength. However, the low ionic conductivity of PVDF limits the

battery performance. Therefore, the application of PVDF leads to high polarization resistance and poor magnification performance. These adverse effects can be reduced by using PVDF-HFP owing to its high ionic conductivity. Kim et.al selected  $\text{UiO}-66(\text{Zr})-(\text{COOH})_2$  (referred to as Zr-based metal-organic framework (Zr-MOF)) and PVDF-HFP to realize an optimized composite AIL.<sup>[146]</sup> The morphology of Zr-MOF80 with the PVDF-HFP coated Zn metal maintained its original structure after cycling, suggesting the formation of dendrite-free of Zn anode. In the case of the Zn symmetric cell coated with the composite AIL, it was confirmed that the cyclability was well-maintained over 2400 cycles at  $10 \text{ mA cm}^{-2}$ , highly superior to the bare Zn

symmetric cell. Fan et al. reported a anion-functionalized interfacial layer composed of sulfonated polyether ether ketone (SPEEK) and UIO-66-SO<sub>3</sub>H.<sup>[147]</sup> Compared with PVDF, SPEEK possesses stronger adhesion abilities due to highly-polar functional groups of -SO<sub>3</sub><sup>-</sup>. Therefore, it adheres closely to the metal plate and binds the Zn<sup>2+</sup> to the metal through hydrogen bonding. Assisted by this AIL, uniform Zn<sup>2+</sup> flux and Zn growth could be established at anode/electrolyte interface. Meanwhile, SPEEK has a low swelling rate and can accommodate the volume expansion of the battery. Based on these advantages of AIL, the symmetric cells present 2400 h cycle life span at a current density of 5 mA cm<sup>-2</sup> and an area capacity of 5 mAh cm<sup>-2</sup>.

### 3.1.2. Inorganic-organic composite AILs synthesized by in-situ

In addition to the ex-situ synthesis of organic-inorganic AILs by coating the pre-synthesized AILs on the surface of Zn anode, in situ formation of inorganic-organic composite AILs is a promising strategy. Admittedly, the in-situ constructing AILs are highly permeable for Zn ions and prevent excess Zn consumption by blocking solvents and electrons. Therefore, in-situ constructing inorganic-organic composite AILs that inherits the merits of each ingredient will open a new avenue to stabilize Zn anode. Some researches focussing on in situ formation of inorganic-organic composite AILs are concluded in Table 2. Importantly, via electrolyte modulation (eutectic,<sup>[148,149]</sup> gel,<sup>[150]</sup> organic<sup>[151]</sup> and hybrid electrolyte,<sup>[41,152]</sup> additives<sup>[153–156]</sup>), additional unusual functionalities can also be obtained, in particular concerning the dendrites suppression and excellent cycling durability for AZIBs.

Compared with traditional electrolytes, eutectic electrolytes have excellent structural flexibility, good thermal/chemical stability, low vapor pressure, and wide potential windows.<sup>[157]</sup> AILs modified Zn anode synthesized via using eutectic electrolyte have been reported in many researches. In 2019, Qiu and his cooperators first fabricated a ZnF<sub>2</sub>/Zn<sup>2+</sup>-permeable organic AIL in-situ with acetamide-Zn(TFSI)<sub>2</sub> eutectic electrolyte. 3D elements distribution of Zn, N, F, and S in the SEI has been identified by time-of-flight secondary-ion mass spectrometry (TOF-SIMS)<sup>[148]</sup> (Figure 7A). As the etching depth increased, the intensity of inorganic compound ZnF<sub>2</sub> gradually increased while those of sulfides and nitrides decreased, indicating that ZnF<sub>2</sub> mainly exists in the inner SEI region and S/N-rich organic compounds are mainly distributed in the outer SEI layer. In this SEI structure, inorganic compound ZnF<sub>2</sub> located in the inner layer guarantee the sufficient mechanical rigidity and the organic components containing S/N located in the outer layer contribute to regulate the solvation structure of Zn<sup>2+</sup>. Thus, the fast ion migration and high mechanical stability of the protective interphase can be realized by this versatile SEI structure. As a result, successfully suppressed HER was achieved by the disappearance of gas production on the surface of SEI-coated Zn (Figure 7B). The as-protected anode exhibited reversible (~100% CE) and dendrite-free Zn plating/stripping even at high areal capacities (>2.5 mAh cm<sup>-2</sup>). Meng et al.

designed an in situ generated gradient organic-inorganic hybrid AIL in a eutectic electrolyte. In this report, eutectic electrolytes consist of hydrated zinc salt Zn(BF<sub>4</sub>)<sub>2</sub>·6H<sub>2</sub>O and solvent DME.<sup>[149]</sup> The organic components were mainly originated from the decomposition of DME, which is ascribed to the protic acid produced by BF<sub>4</sub><sup>-</sup> hydrolysis attacking the O containing lone pair electrons in the DME molecules. The dense inorganic ZnF<sub>2</sub> passivation layer effectively isolated water from contact with Zn anode, inhibiting the further formation of the passivation layer and the HER.

The in-situ organic-inorganic AILs can also be realized by the regulation of the gel electrolyte.<sup>[150]</sup> As reported, a zinc-anode-compatible in situ organic-inorganic AIL was formed in Zn(ClO<sub>4</sub>)<sub>2</sub> salt hydrogel electrolyte (denoted ADC-gel electrolyte) modulation (Figure 7C). In this case, the surface composition on Zn anode was synergistically functionalized with polyzwitterionic groups and a thin reduction layer formed after several cycles (Figure 7D), which was determined by XPS analysis. As a result, the uniform and flat Zn deposition can be clearly observed in the ADC-gel electrolyte-based cell at the current of 4 mA within 20 min compared with that in the common liquid electrolyte (Figure 7E).

Organic molecules, with a small highest occupied molecular orbital-lowest unoccupied molecular orbital (HOMO-LUMO) energy level, can act as a sacrifice ingredient to form a SEI layer during the first few cycles, thus providing dynamic protection against excessive depletion of Zn stocks.<sup>[158]</sup> In addition to gel electrolyte, organic electrolyte can also alleviate the dendrite of Zn anodes by in-situ constructing organic-inorganic composite AILs (Figure 7F).<sup>[151]</sup> For instance, a hybrid interphase consisting of an organic-rich outer layer and an inorganic inner layer (Zn<sub>3</sub>(PO<sub>4</sub>)<sub>2</sub>–ZnF<sub>2</sub>–ZnS) was generated in the triethyl phosphate solvent and trifluoromethanesulfonate anion (OTF<sup>-</sup>) reduction decomposition. By putting bare Zn and AIL–Zn into aqueous Zn(OTF)<sub>2</sub>-based electrolytes, the presence of the AIL can significantly suppress the formation of by-product (Figure 7G).

Hybrid electrolytes are another potential way to construct in-situ organic-inorganic composite AILs. Li et.al designed a low-concentration aqueous Zn(OTF)<sub>2</sub>–Zn(NO<sub>3</sub>)<sub>2</sub> electrolyte to in situ form a robust inorganic (ZnF<sub>2</sub>–Zn<sub>5</sub>(CO<sub>3</sub>)<sub>2</sub>–(OH)<sub>6</sub>)-organic bilayer AIL, where the inorganic inner layer promotes Zn-ion diffusion while the organic outer layer suppresses water penetration.<sup>[41]</sup> As shown in Figure 8(A), Zn<sub>5</sub>(OH)<sub>8</sub>(NO<sub>3</sub>)<sub>2</sub>·2H<sub>2</sub>O passivation layer is formed via a series of the chemical reactions. As an intermediate template layer, Zn<sub>5</sub>(OH)<sub>8</sub>(NO<sub>3</sub>)<sub>2</sub>·2H<sub>2</sub>O gradually transforms into a more stable Zn-ion conductive Zn<sub>5</sub>(CO<sub>3</sub>)<sub>2</sub>(OH)<sub>6</sub> layer. At the same time, the flexible organic components form as out-layer via the reaction between (CF<sub>3</sub>SO<sub>3</sub>)<sup>-</sup> and NO<sub>3</sub><sup>-</sup>, in which the zinc ion conducting ZnF<sub>2</sub> forms in the inner part. It is also reported that a method of preconditioning of a zinc anode in hybrid electrolytes (based on poly(ethylene glycol)-200 and H<sub>2</sub>O) can also prepare an organic-inorganic composite AIL.<sup>[152]</sup> Consequently, the AIL–Zn delivered a reversible Zn plating/stripping CE to 99.23% (average of 1300 cycles) and maintained uniform Zn<sup>2+</sup> flux at wide temperature ranges (from –20 to 40 °C).

Composite Alls	Protection mechanism	Fabricating method	Hysteresis voltage	Cyclic lifespan	Ref.
ZnF <sub>2</sub> –ZnSO <sub>3</sub> –ZnCO <sub>3</sub> /polymeric framework (400–500 nm)	Physical isolation barrier; Optimize nucleation barrier	Electrolyte addition	80 mV	Over 6,000 cycles at 0.5 mAcm <sup>-2</sup> and 0.25 mAhcm <sup>-2</sup>	[155]
ZnF <sub>2</sub> –S–N-rich/organic components (64 nm)	Physical isolation barrier; Optimize nucleation barrier	Eutectic electrolyte	78 mV	Over 1000 cycles at 0.1 mAcm <sup>-2</sup>	[148]
Zn <sub>4</sub> SO <sub>4</sub> (OH) <sub>6</sub> /Zn (Hmim) <sup>[a]</sup>	Optimize nucleation barrier; Physical isolation barrier	Electrolyte addition	–	800 h at 2 mAcm <sup>-2</sup> and 2 mAhcm <sup>-2</sup>	[156]
Zn <sub>3</sub> (PO <sub>4</sub> ) <sub>2</sub> –ZnF <sub>2</sub> –ZnS/organic components	Physical isolation barrier; Optimize nucleation barrier	Organic electrolyte	80 mV	over 2500 h at 1 mAcm <sup>-2</sup> and 1 mAhcm <sup>-2</sup>	[151]
ZnF <sub>2</sub> –Zn <sub>5</sub> (CO <sub>3</sub> ) <sub>2</sub> (OH) <sub>6</sub> /organic components	Regulate Zn <sup>2+</sup> solvation structure; Physical isolation barrier	Hybrid electrolyte	20 mV	over 1200 h at 0.5 mAcm <sup>-2</sup> and 0.5 mAhcm <sup>-2</sup>	[41]
LDH <sup>[b]</sup> /organism of PEG <sup>[d]</sup> /composite	Regulate Zn <sup>2+</sup> solvation structure; Physical isolation barrier	Hybrid electrolyte	20 mV	over 1000 h at 1 mAcm <sup>-2</sup> and 1 mAhcm <sup>-2</sup>	[152]
ZnF <sub>2</sub> –ZnS-rich/organic components	Regulate Zn <sup>2+</sup> solvation structure; Physical isolation barrier	Electrolyte addition	90 mV	over 5000 h at 2 mAcm <sup>-2</sup> and 1 mAhcm <sup>-2</sup>	[154]
Inorganic Cl <sup>-</sup> containing layer/polar functional groups (–NH <sub>2</sub> –SO <sub>3</sub> <sup>-</sup> )	Homogenize the Zn <sup>2+</sup> flux; Physical isolation barrier	Gel electrolyte	50 mV	1700 h at 1 mAcm <sup>-2</sup> and 1 mAhcm <sup>-2</sup>	[150]
ZnS–ZnCO <sub>3</sub> –ZnSO <sub>3</sub> /BBI <sup>[d]</sup> -derivate (SO <sub>2</sub> NSO <sub>2</sub> <sup>-</sup> )	Regulate Zn <sup>2+</sup> solvation structure; Homogenize the Zn <sup>2+</sup> flux; Optimize nucleation barrier	Electrolyte addition	100 mV	over 5000 h at 0.5 mAcm <sup>-2</sup> and 0.5 mAhcm <sup>-2</sup>	[153]

[a] Hmim refers to 2-methyl imidazole. [b]: LDH refers to the mixture of zinc hydroxylchloride-zinc hydroxycarbonate. [c]: PEG is the abbreviation of poly(ethylene glycol)-200. [d] BBI refers to a dibenzene sulfonamide electrolyte addition.

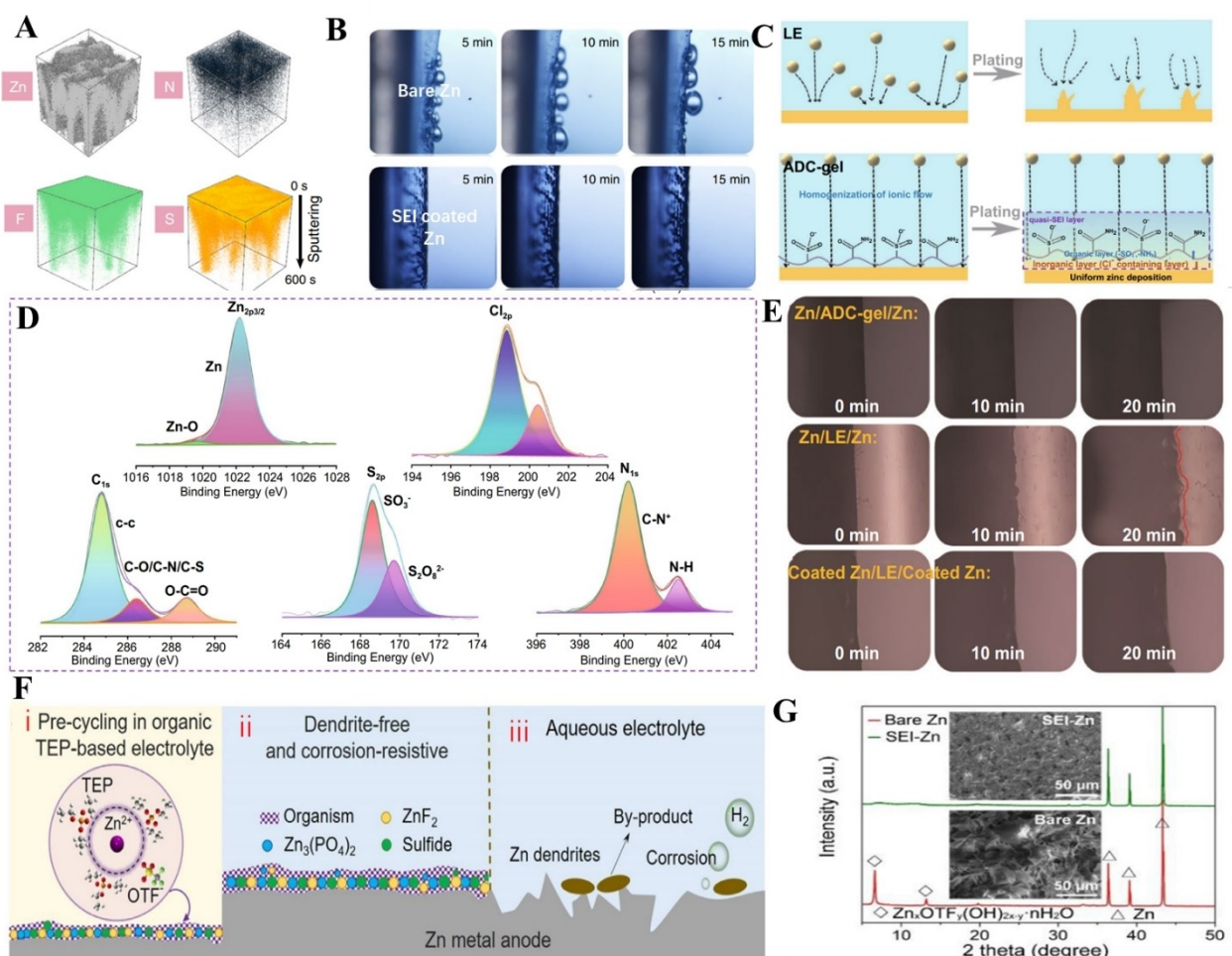


**Figure 7.** A) Three-dimensional view of Zn, N, F, and S elements distributions of SEI in the time-of-flight secondary-ion mass spectrometry (TOF-SIMS) sputtered volumes. B) In situ investigations of the Zn deposition by optical microscopy in Zn/Zn cells. Reproduced from ref. [148]. Copyright (2022), with permission from Elsevier Ltd. C) Schematic illustration of the Zn deposition on the anode surface in different electrolytes. LE refers to liquid electrolyte. ADC-gel refers to gel electrolyte with  $Zn(ClO_4)_2$  salt. D) High-resolution XPS spectra of the surface of the cycled Zn anode. E) In-situ optical microscope observing the Zn deposition at a voltage of 4 mV in Zn//Zn symmetric cells to investigate the validity of SEI layer. Reproduced from ref. [150]. Copyright (2022), with permission from Springer Nature. F) Function and characterization of the organic-inorganic hybrid interphase on Zn. Schematic illustration of (i) the formation of hybrid SEI on Zn electrode in the TEP-based electrolyte and the surface chemistry on (ii) SEI-Zn and (iii) bare Zn electrodes in aqueous electrolytes. G) XRD patterns and SEM images (insets) of bare Zn and SEI-Zn electrodes soaked in aqueous electrolytes for 24 h. Reproduced from ref. [151]. Copyright (2022), with permission from Elsevier Ltd.

Adding electrolyte additives is the simplest and commonest method to construct inorganic-organic AIL by in situ. For instance, a complex fluorinated interphase was in situ fabricated on Zn anode via adding trimethylethyl ammonium trifluoromethanesulfonate alkylammonium salt ( $Me_3EtN^{+}OTF^{-}$ ) into  $Zn(OTF)_2$ -based aqueous electrolyte (Figure 8B).<sup>[155]</sup> The formed  $ZnF_2$ -riched interface phase has been proved to facilitate the rapid diffusion of  $Zn^{2+}$  beyond the physically shielding the free water molecules on the Zn surface. Meanwhile, the high interface energy at  $ZnF_2/Zn$  interface could promote the horizontal rather than vertical migration and deposition of  $Zn^{2+}$ , indicating the critical role in restricting the growth of Zn dendrites. As shown by Figure 8(C), the Zn electrode with  $Me_3EtN^{+}OTF^{-}$  electrolyte additive had a smooth and compact surface structure after a long cyclic test. In contrast, the Zn electrode without

$Me_3EtN^{+}OTF^{-}$  electrolyte additive showed abundant dendrites and cracks.

In addition, Wu et.al introduced 2-methyl imidazole (Hmim) as an electrolyte additive to in-situ construct a robust inorganic-organic Zn-rich (consist of  $Zn_4SO_4(OH)_6/Zn$  (Hmim)) composite AIL for realizing the multifunction of AIL.<sup>[156]</sup> On the one hand, the zincophilic properties of Hmim and its chelation with  $Zn^{2+}$  result in more active sites for initial nucleation, leading to the uniform zinc deposition, and the change of coordination environment makes the diffusivity of ions decrease and the nucleation overpotential increase, which result in smaller grains in the initial zinc deposition stage. The nucleation overpotential of blank electrolyte is 27 mV, the Hmim-based electrolyte (Hmim concentration-0.025 mol L<sup>-1</sup>) is 43 mV (Figure 8D). Larger nucleation barrier contributes to more uniform  $Zn^{2+}$  deposition. On the other hand, the as-formed  $Zn_4SO_4(OH)_6 \cdot 3H_2O$  will coat

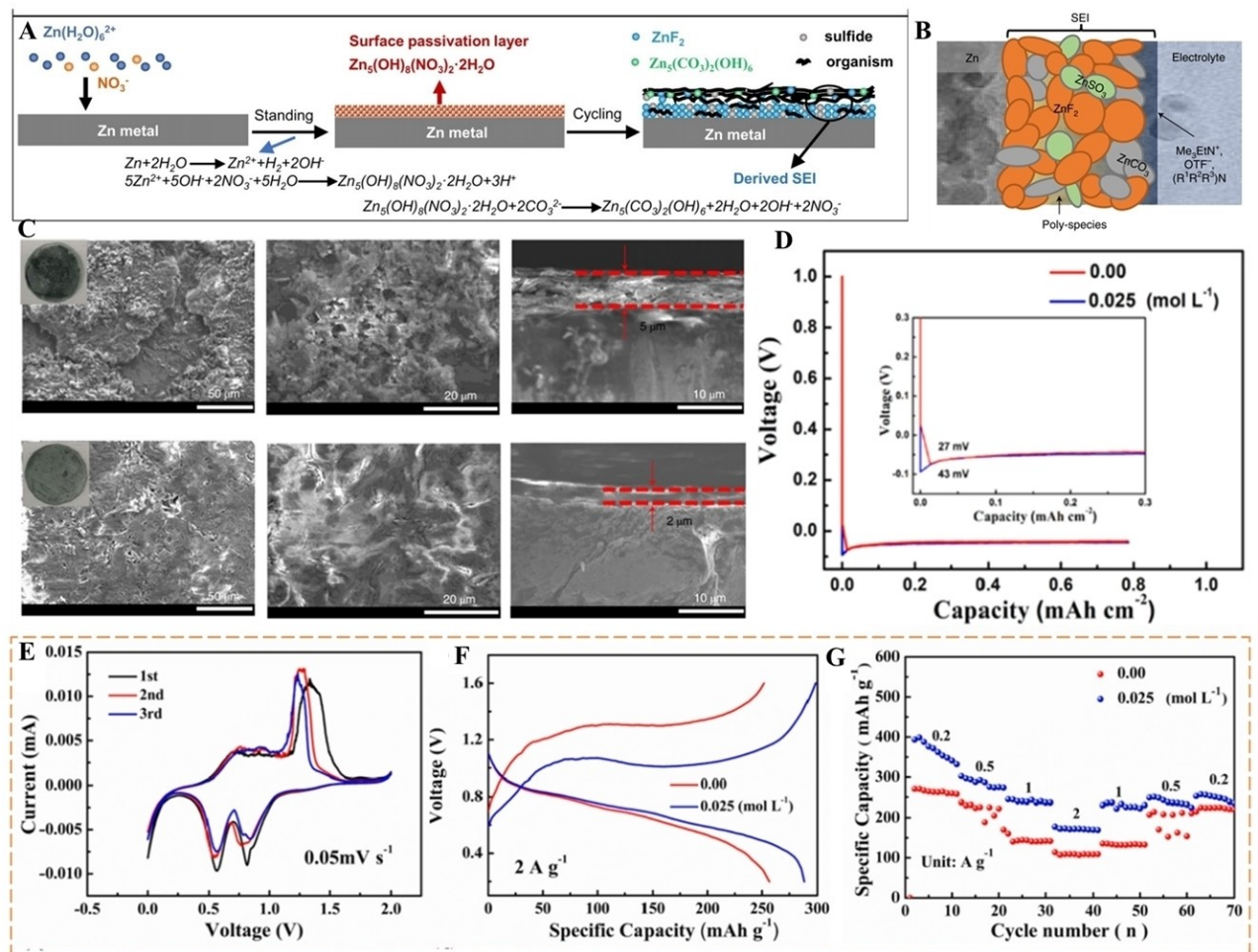


**Figure 8.** A) Formation mechanism of  $\text{ZnF}_2\text{-Zn}_5(\text{CO}_3)_2(\text{OH})_6$ -organic SEI in aqueous zinc trifluoromethanesulfonate ( $\text{Zn}(\text{OTF})_2$ ) electrolyte with  $\text{Me}_3\text{EtNOTF}$  as an additive. The presence of  $\text{NO}_3^-$  promotes the formation of an electrically and ionically insulating  $\text{Zn}_5(\text{OH})_8(\text{NO}_3)_2\cdot 2\text{H}_2\text{O}$  layer (red), which subsequently transforms into an electrically insulating but ionically conductive SEI in which the  $\text{ZnF}_2\text{-Zn}_5(\text{CO}_3)_2(\text{OH})_6$  inner part is coated by the organic outer part. Reproduced from ref. [41]. Copyright (2021), with permission from Wiley. B) Cartoon of  $\text{Zn}^{2+}$ -conducting SEI after adding  $\text{Me}_3\text{EtNOTF}$  electrolyte additive.  $\text{Me}_3\text{EtNOTF}$  = trimethylylethyl ammonium trifluoromethanesulfonate. C) SEM images after 50 plating/stripping cycles with and without  $\text{Me}_3\text{EtNOTF}$  electrolyte additive (Up: with  $\text{Me}_3\text{EtNOTF}$ ; down: without  $\text{Me}_3\text{EtNOTF}$ ). Reproduced from ref. [155]. Copyright (2022), with permission from Springer Nature. D) The plating profile of Zn/Zn symmetrical cells in  $\text{ZnSO}_4$  electrolyte and  $\text{ZnSO}_4$  electrolyte with Hmim additive. Hmim refers to 2-methyl imidazole. E–G) Electrochemical performance of full cells with and without Hmim additive: E) CV curves of Zn |  $\text{V}_2\text{O}_5$  cell tested at the scan rate of  $0.05 \text{ mV s}^{-1}$ . F) Galvanostatic charge/discharge curves of Zn |  $\text{V}_2\text{O}_5$  at the current density of  $2 \text{ A g}^{-1}$ . G) Rate performance of Zn |  $\text{V}_2\text{O}_5$  cells. Reproduced from ref. [156]. Copyright (2023), with permission from Elsevier Ltd.

on the Zn anode and then participate in the formation of SEI film, which will inhibit the intimate contact of anode with electrolyte, thus effectively relieve the chemical corrosion. Consequently, the composite AIL-protected Zn anode has good chemical and thermal stability properties, and both the side reactions and Zn dendrites can be effectively inhibited (Figure 8E–G).

### 3.2. Inorganic-inorganic composite AILs

#### 3.2.1. Inorganic-inorganic composite AILs synthesized by ex-situ

Constructing inorganic-inorganic composite AILs synthesized by ex-situ is also an effective approach to stable Zn anode. Some relevant researches are summarized in Table 3. Cu substrate is

commonly used as a current collector due to the alloying reaction which reduces nucleation overpotential, regulates uniform  $\text{Zn}^{2+}$  flux and ultimately inhibits Zn dendrites. However, those messy and big pores architecture in conventional copper foam results in uneven local current distribution and unsatisfactory consumption of electrolyte, which further triggers poor ion transfer and disordered  $\text{Zn}^{2+}$  flux near the surface of substrates, thus leading to the inhomogeneous and dendritic Zn deposition.<sup>[159]</sup> Many effective interfacial engineering strategies have been developed to design a multifunctional AILs containing the component of Cu (nanosheets, nanoparticles).

For example, Sun et al. synthesized a composite AIL consisting of Cu nanosheets and GO (Cu–GO) (Figure 8A).<sup>[160]</sup> GO with low conductivity can inhibit the parasitic reaction between electrolyte and Zn electrode and avoid the generation of by-products and electrolyte consumption. The thin GO layer

**Table 3.** Summary of Inorganic-inorganic composite AILs by ex-situ for improving Zn metal anode.

Composite AILs	Protection mechanism	Fabricating method	Hysteresis voltage	Cyclic Lifespan	Ref.
Cu/GO <sup>[a]</sup>	Homogenize the $Zn^{2+}$ flux; Optimize nucleation barrier;	Spin coating	–	2000 h at $0.5 \text{ mA cm}^{-2}$ and $0.5 \text{ mAh cm}^{-2}$	[160]
Cu/CF	Optimize nucleation barrier; Uniform electrical field	Blade coating	58 mV	over 2200 h at $1.0 \text{ mA cm}^{-2}$ $1.0 \text{ mAh cm}^{-2}$	[60]
Cu-Ps/EG <sup>[b]</sup>	Physical isolation barrier; Uniform electrical field; Optimize nucleation barrier	Electrodeposition	142.8 mV	over 3000 h at $10.0 \text{ mA cm}^{-2}$ and $10.0 \text{ mAh cm}^{-2}$	[164]
AlN/Ag <sup>[c]</sup> 1.4–1.6 $\mu\text{m}$	Uniform electrical field; Regulate $Zn^{2+}$ solvation structure; Homogenize the $Zn^{2+}$ flux	Sputtering	$\approx 46 \text{ mV}$	2600 h at $1 \text{ mA cm}^{-2}$ and $1 \text{ mAh cm}^{-2}$	[165]
LCNF <sup>[d]</sup> /MXene 48 $\mu\text{m}$	Homogenize the $Zn^{2+}$ flux; Uniform electrical field; Regulate $Zn^{2+}$ solvation structure	Blade coating	35 mV	788 h at $1 \text{ mA cm}^{-2}$ and $1 \text{ mAh cm}^{-2}$	[167]
Ag/Ni/NiO $\approx 280 \mu\text{m}$	Homogenize the $Zn^{2+}$ flux; Regulate $Zn^{2+}$ solvation structure	Electrodeposition	17 mV	400 h at $5 \text{ mA cm}^{-2}$ / $2.5 \text{ mAh cm}^{-2}$	[168]
ZnF <sub>2</sub> /Ag	Homogenize the $Zn^{2+}$ flux; Optimize nucleation barrier	Displacement reaction	$\approx 18 \text{ mV}$	2200 h at $2 \text{ mA cm}^{-2}$ and $2 \text{ mAh cm}^{-2}$	[166]
Cu/CNFs <sup>[e]</sup>	Homogenize the $Zn^{2+}$ flux; Regulate $Zn^{2+}$ solvation structure	Dip-coating	14.6 mV	2200 h at 0.5 and $0.25 \text{ mAh cm}^{-2}$	[161]
Cu/ZnF <sub>2</sub>	Homogenize the $Zn^{2+}$ flux; Optimize nucleation barrier	Solution dipping	76 mV	2000 hours at $1 \text{ mA cm}^{-2}$ and $1 \text{ mAh cm}^{-2}$	[173]

[a] GO is the abbreviation of graphene oxide; [b] Cu-Ps refers to in-situ formed copper particles. EG refers to expanded graphite; [c] AlN/Ag refers to a silver (Ag) nanoparticle embedded amorphous AlN matrix protective layer on Zn anodes; [d] LCNF refers to lignin-containing cellulose nanofiber. LM=(LCNF)-Mxene; [e] CF refers to a stable fluorine-doped amorphous carbon artificial layer constructed on a Cu current collector.

also improves the hydrophilicity with polar groups. The Cu nano-layer adjacent to GO can enhance the  $Zn^{2+}$  transfer kinetic and dramatically decrease the nucleation barrier due to the abundant zincophilic sites. As a result, the lifespan of the coated Zn symmetric cell was extended to over 2000 h at  $0.5 \text{ mA cm}^{-2}/0.5 \text{ Ah cm}^{-2}$ .

Except the above-mentioned Cu-GO composite layer, a fluorine-doped amorphous carbon nanofibers (CF) interfacial layer on Cu current collector (CF-Cu) was proposed.<sup>[161]</sup> Amorphous carbon not only has high mechanical strength, but also has superior ionic conductivity and electronic insulation properties, which is conducive to improve ionic diffusion ability and interface stability. According to this, CF with highly dispersed zincophilic Cu nanoparticles (Cu-NPs) as a composite AIL was investigated to realize dendrite-free Zn anode.<sup>[60]</sup> Figure 8(B) showed the strongest adsorption of Zn(002), Zn-(100), and Zn(101) on CF compared with Cu and C, indicating a strong interaction of CNFs with Zn. The adsorption of Zn(002) to CNFs is better than that of Zn(100) and Zn(101) on CF surface. In contrast, for Cu and C surface, the preferred adsorption surface is Zn(101). Correspondingly, the CF-Cu@Zn |  $\text{V}_2\text{O}_5$  full battery exhibited a high initial specific discharge capacity of  $\approx 370 \text{ mAh g}^{-1}$  followed by a prolong steady cycling (Figure 8C).

Among all carbonaceous materials, expanded graphite (EG) has attracted much attention because of its large interlayer between carbon layers to facilitate the insertion and desorption of  $Zn^{2+}$ .<sup>[162]</sup> EG should not only have the ability to block the

growth of Zn dendrites by guiding the epitaxial electrodeposition of Zn, similar to graphene substrate, but also have a very high cost-benefit advantage compared with other nano-carbon.<sup>[163]</sup> Chen and his cooperators proposed a dendrite-free and flexible substrate (denoted Cu/EG) for Zn metal anode that is composed of in-situ formed Cu particles embedded on the graphite nanosheets of EG (Figure 8D).<sup>[164]</sup> Cu nanoparticles can reduce the nucleation overpotential of Zn due to their affluent zincophilic sites and the tight link of Cu particles to the neighboring graphite sheets contributed to stabilize the AIL structure. Simultaneously, the EG can induce the epitaxial electrodeposition of Zn over the graphite surface to offer the Zn uniform deposition (Figure 8D). Zn//Zn symmetric cells equipped with this anode showed low deposition overpotentials ( $22.0/142.8 \text{ mV}$  @  $1.0/10.0 \text{ mA cm}^{-2}$ ) and ultralong lifespan over 3000 h at  $10.0 \text{ mA cm}^{-2}$  and  $10.0 \text{ mAh cm}^{-2}$  (Figure 8E).

Except the above-mentioned Cu-based composite layer, Ag-based materials as the protective layer of Zn anode can also reduce the nucleation overpotential of Zn due to the alloying reaction. Zheng et al. applied a reactive magnetron sputtering method to deposit Ag nanoparticles embedded amorphous aluminum nitride (AlN/Ag) protective layer on the surface of Zn foils.<sup>[165]</sup> The well-distributed zincophilic Ag nanoparticles would react with Zn in situ during cycling to form  $\text{AgZn}_3$  sites (Figure 8F), facilitating the homogeneous distribution of electric field and  $Zn^{2+}$  and the following Zn (002) growth. Multiphysics simulations identify the even electric and ionic fields on the AlN/Ag@Zn anode (Figure 8G). Amorphous AlN can play a

buffering role in adapting to the volume expansion of Zn anode during cycle. The lifespan of the symmetric cells prolonged to 2600 h for AlN/Ag@Zn electrodes. Besides, a composite AIL composed of  $ZnF_2$  and Ag as a model of hybrid surfaces on Zn was also developed.<sup>[166]</sup> Figure 8(H) summarizes the protection principle of  $ZnF_2$ -Ag composite AIL in Zn plating process. Similarly, Ag can form stable  $AgZn_3$  alloy with Zn to promote the electroplating process and inhibit the HER due to its high overpotential towards HER. Hydrophobic  $ZnF_2$  has a small diffusion barrier of  $Zn^{2+}$  which is beneficial to accelerate the transportation of  $Zn^{2+}$ .

Liu and his cooperators fabricated a novel lignin-containing cellulose nanofiber (LCNF)-MXene (LM) protective layer enabling long-cycle-life Zn//Zn symmetrical batteries.<sup>[167]</sup> On the one hand, LCNF provided sufficient mechanical strength (43.7 MPa) at relatively low porosity (52.2%) to achieve diffusion limited dendrite suppression. On the other hand, MXene, as a Zn gate layer, could promote the  $Zn^{2+}$  migration, limits the degradation of active water/anions at the electrode/electrolyte interface, and epitaxial guides the deposition of Zn along the (002) plane. To evaluate the effect of the LM layer on parasitic reactions of Zn anode, the discharge capacities of the fully charged cells (rest for 48 h) were measured (Figure 9A).

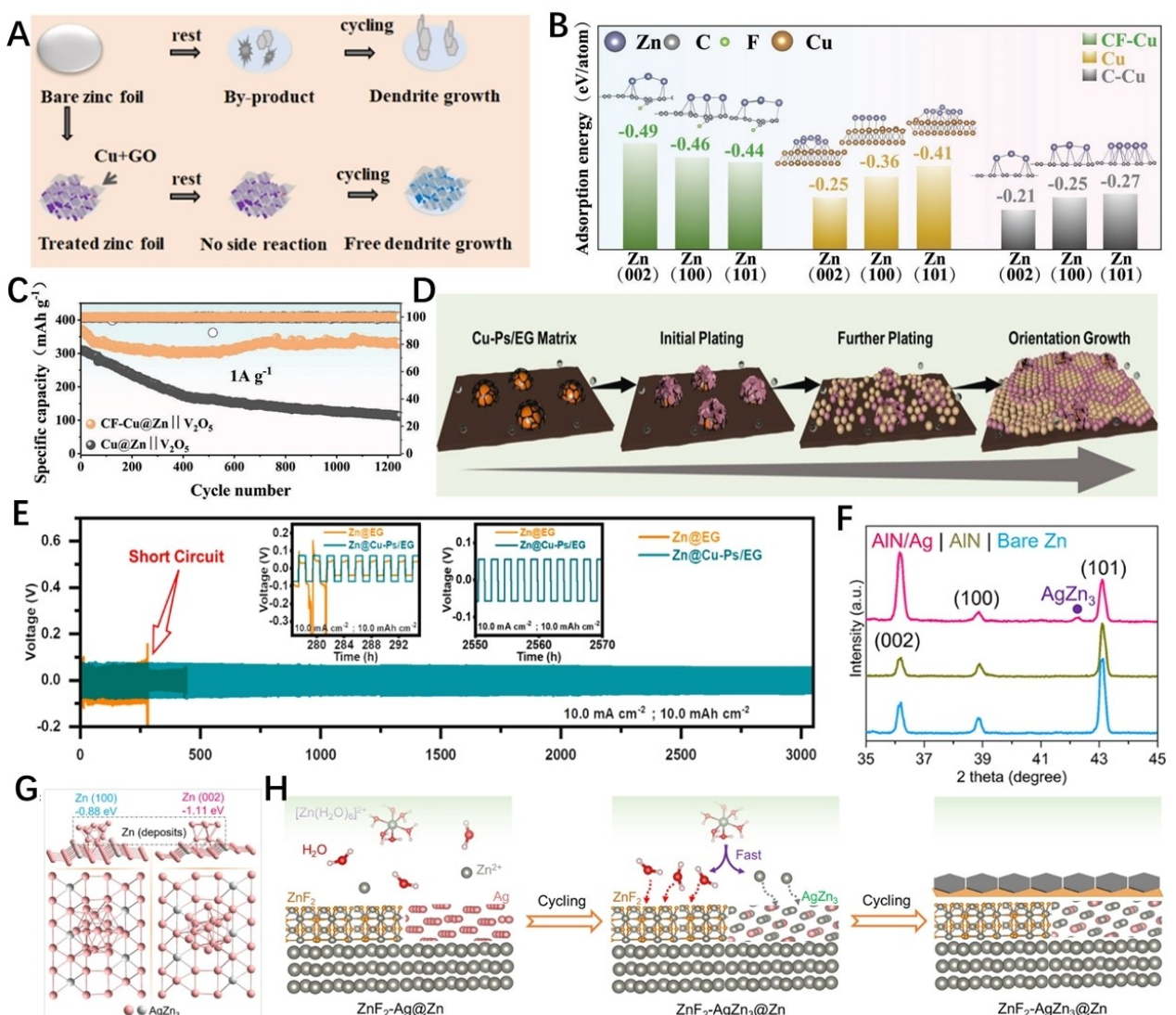


**Figure 9.** A) Schematic diagram of the Zn deposition evolution on bare Zn (up) and treated Zn with Cu-GO (down). GO refers to graphene oxide. Reproduced from ref. [160]. Copyright (2022), with permission from American Chemical Society. B) Adsorption energy of Zn(002), Zn(100), Zn(101) on CF, C and Cu(111). CF refers to a stable fluorine-doped amorphous carbon artificial layer is constructed on a Cu current collector. C) Long-term cycling of CF-Cu@Zn |  $V_2O_5$  and Cu@Zn |  $V_2O_5$  cells at 1  $\text{A g}^{-1}$  in  $ZnSO_4$  electrolyte. Reproduced from ref. [161]. Copyright (2022), with permission from Wiley-VCH. D) The schematic illustrations of Zn deposition on Cu-Ps/EG matrix. Cu-Ps refers to in-situ formed copper particles. EG refers to expanded graphite. E) The plating and stripping cycle of EG and Cu-Ps/EG matrixes at 10.0  $\text{mA cm}^{-2}$  with a capacity of 10.0  $\text{mAh cm}^{-2}$  in 3 M  $Zn(CF_3SO_3)_2$  aqueous electrolyte. Reproduced from ref. [164]. Copyright (2022), with permission from Elsevier Ltd. F) XRD patterns of various Zn anodes after long cycling. AlN/Ag refers to a silver (Ag) nanoparticle embedded amorphous AlN matrix protective layer on Zn anodes. Reproduced from ref. [165]. Copyright (2023), with permission from American Chemical Society. G) Binding energies of Zn (002) and Zn (100) on AgZn<sub>3</sub> (101) sites. H) Schematic illustration of Zn deposition on ZnF<sub>2</sub>-Ag@Zn during cycles in  $ZnSO_4$  electrolyte. Reproduced from ref. [166]. Copyright (2022), with permission from American Chemical Society.

Approximately 81.7% of the original capacity was retained in the Zn-LM//MnO<sub>2</sub> cell exceeding 70.1% in the Zn//MnO<sub>2</sub> cell, which imply the effective suppression of the side-reactions by the LM layer.

At present, there are many researches focus on multi-gradient one/two/three gradient AILs. Take three-gradient AIL as example, Gao et al. synthesized an Ag/Ni/NiO three-gradient AIL to optimize the Zn anode.<sup>[168]</sup> In this design, a the conductive zincophilic material Ag was used as the bottom layer, NiO semiconductor was used as top layer with poor Zn affinity, and metal Ni was studied as the intermediate layer between Ag and NiO. Thus, this AIL integrated the advantages of gradient conductivity, Zn affinity and porosity (Figure 9B) and the final element simulations of triple-gradient electrodes are shown in the Figure 9(C). Due to the high zincophilia of Ag, the bottom part was the first choice for Zn deposition and the bottom-up deposition behavior was conducive to realizing a uniform Zn deposition. After cycling for a while, the surface of the non-gradient Zn anode is rough and had obvious protrusions and pits. However, the Zn deposition on the surface of the three-gradient electrode was flat and uniform.

### 3.2.2. Inorganic-inorganic composite AILs synthesized by *in-situ*

Most of inorganic coating materials are generally rigid and less viscous. Therefore, the ex-situ generated protective layers may easily be detached from the Zn surface due to the volume change during cycling. In view of this situation, *in-situ* synthesis coating has been reported as interface layer to stabilize Zn anode. Commonly, adding applicable electrolyte additives is a facile method to form *in-situ* multifunctional inorganic-inorganic AILs to solve non-uniform Zn deposition (Table 4).

In 2020, Cao et al. first fabricated a Zn<sub>12</sub>(SO<sub>4</sub>)<sub>3</sub>Cl<sub>3</sub>(OH)<sub>15</sub>·5H<sub>2</sub>O-ZnSO<sub>3</sub>-ZnS inorganic-inorganic composite AIL by *in-situ* in ZnCl<sub>2</sub>H<sub>2</sub>O-DMSO electrolyte.<sup>[169]</sup> The addition of DMSO leads to less electron transfer between Zn and O in H<sub>2</sub>O or DMSO, thereby weakening the bonding strength between Zn<sup>2+</sup> and H<sub>2</sub>O in the Zn<sup>2+</sup> solvation sheath. In addition, the preference reduction of DMSO during Zn deposition forms a dense Zn<sub>12</sub>(SO<sub>4</sub>)<sub>3</sub>Cl<sub>3</sub>(OH)<sub>15</sub>·5H<sub>2</sub>O-ZnSO<sub>3</sub>-ZnS solid electrolyte interphase, inhibiting the decomposition of solvated H<sub>2</sub>O.

Recently, Cao et.al successfully *in situ* constructs a Zincophilic/Zincophobic Sn/Zn<sub>5</sub>(OH)<sub>8</sub> Cl<sub>2</sub>·H<sub>2</sub>O bilayer interphase by introducing additive into eutectic 0.05 M SnCl<sub>2</sub> and 7.6 M ZnCl<sub>2</sub> aqueous electrolyte (Figure 9D).<sup>[170]</sup> The Zn solvent sheath structure in aqueous electrolyte is Zn(H<sub>2</sub>O)<sub>6</sub>. In high concentrated ZnCl<sub>2</sub> electrolyte, the strongly interaction of Cl<sup>-</sup> and Zn<sup>2+</sup> can give rise to the replacement of H<sub>2</sub>O by Cl<sup>-</sup> in Zn<sup>2+</sup> solvation sheath and thus to weaken the activity of free water. Meanwhile, hydrogen bond interactions between H<sub>2</sub>O and Cl<sup>-</sup> decreased water activity. Besides, a Zincophilic Sn layer could be deposited on the Zn surface *in situ*, which promoted the formation of Zincophobic Zn<sub>5</sub>(OH)<sub>8</sub>Cl<sub>2</sub>H<sub>2</sub>O layer and further uniformized the Zn<sup>2+</sup> flux. The combination of reduced water activity and Zincophilic-Zincophobic interfacial bilayer enabled

Ref.	Composite AILs	Protection mechanism	Fabricating method	Hysteresis voltage	Cyclic Lifespan	
[169]	Zn <sub>12</sub> (SO <sub>4</sub> ) <sub>3</sub> Cl <sub>3</sub> (OH) <sub>15</sub> ·5H <sub>2</sub> O-ZnSO <sub>3</sub> -ZnS	Homogenize the Zn ion flux; Regulate Zn ion solvation structure; Optimize nucleation barrier	Eutectic electrolyte	≈ 8 mV	≈ 500 h at 3 mA cm <sup>-2</sup> and 3 mAh cm <sup>-2</sup>	1000 h at 0.5 mA cm <sup>-2</sup> and 0.5 mAh cm <sup>-2</sup>
[170]	Sn/Zn <sub>5</sub> (OH) <sub>8</sub> Cl <sub>2</sub> ·H <sub>2</sub> O	Regulate Zn ion solvation structure; Optimize nucleation barrier	Chemical reaction	≈ 50 mV	1200 h at 2 mA cm <sup>-2</sup> and 4 mAh cm <sup>-2</sup>	
[171]	Zn <sub>5</sub> Po <sub>4</sub> /ZnF <sub>2</sub>	Regulate Zn ion solvation structure; Uniform electrical field	Electrolyte addition	25 mV		

dendrite-free Zn plating/stripping to achieve a high CE of 99.7% for  $> 500$  h.

Additionally, other electrolyte additives such as KPF<sub>6</sub> have also been shown to be effective in the in-situ synthesis of inorganic-inorganic composite AIL.<sup>[171]</sup> The composite AIL are composed of Zn<sub>3</sub>(PO<sub>4</sub>)<sub>2</sub> and ZnF<sub>2</sub> (ZCS) with versatile functions. Zn<sub>3</sub>(PO<sub>4</sub>)<sub>2</sub> with ultra-high interface energy towards Zn substrate possesses great potential in suppressing Zn dendrite growth and ZnF<sub>2</sub> boasts unique merits in the kinetics of Zn<sup>2+</sup> transference and deposition. With the assistance of the in situ ZCS layer, Zn||Zn symmetrical cells showed excellent plating/stripping reversibility and cycling stability (Figure 9E).

The ZnF<sub>2</sub> interface layer with good ionic conductivity and low electronic conductivity can be constructed by gas-solid reaction in-situ. It has been considered as the best protective coating for Zn anode at present. In order to further improve the electrochemical performance of ZnF<sub>2</sub> protected Zn anode, cooperating with Cu, a strong Zincophilic metal, has been considered to be an effective strategy.<sup>[146,172–173]</sup> Liang et al. successfully synthesized gradient fluorinated alloying (GFA) composite AIL by combining 3D metal alloy with electronic insulating ZnF<sub>2</sub> on the Zn anode surface for the first time.<sup>[173]</sup> The GFA coating was formed in situ on the Zn metal foil through a simple solution-dipping approach, of which ZnF<sub>2</sub> distributed in the outer layer and CuZn alloy located in the inner layer, (Figure 9F). The formation mechanism of GFA particles are as follows: (1) Zn + CuF<sub>2</sub> → ZnF<sub>2</sub> + Cu, (2) 0.61 Cu + 0.39 Zn → Cu<sub>0.61</sub>Zn<sub>0.39</sub>. Electron-insulating and hydrophobic ZnF<sub>2</sub> could prevent direct electron transfer between water and Zn while the formed alloy layer provided plenty of Zn plating space. Designed AIL protected Zn electrodes delivered a stable plating/stripping cycling life for 700 hours with a cycled areal capacity of 3 mAh cm<sup>-2</sup> at 3 mA cm<sup>-2</sup>.

### 3.3. Organic-organic Composite AILs

Akin to organic-inorganic and inorganic-inorganic interface AILs, a series of researches regarding the organic-organic composite AILs have been conducted in consideration of respective characteristics of different organic materials possessing, including good flexibility and excellent adaptability towards volume changes of Zn electrode (Table 5).

An organic-organic AIL consist of glutinous carboxymethyl cellulose (CMC) and amorphous porous covalent organic polymers (COPs) skeleton was constructed by Ding et al. as a multifunctional coating layer for Zn anode (Figure 10A).<sup>[174]</sup> The abundant hydrophilic hydroxyl and carboxyl groups in CMC as are favorable to the formation of quasi-gel composite.<sup>[175]</sup> Impressively, the transport mechanism of Zn<sup>2+</sup> is altered to a faster and more stabilized hopping mechanism by virtue of the ionic dipole interaction and Coulombic attraction force between Zn<sup>2+</sup> and the hydrophilic groups in CMC. Besides, nano-porous COPs could serve as a rigid skeleton to accommodate the volume change during repetitive Zn plating/stripping. The multifunctional quasi gel layer with high Zn<sup>2+</sup> conductivity was designed in situ by putting the COP-CMC-coated Zn electrode

Composite AILs	Protection mechanism	Fabricating method	Hysteresis voltage	Cyclic Lifespan	Ref.
PA <sup>[a]</sup> /Zn(TFO) <sub>2</sub>	Optimize nucleation barrier; Physical isolation barrier	Blade coating	–	Over 1500 h at 0.2 mA cm <sup>-2</sup> and 0.1 mAh cm <sup>-2</sup>	[177]
COP-CMC/QG <sup>[b]</sup>	Homogenize the Zn ion flux; Optimize nucleation barrier	Blade coating	28 mV	over 4000 h at 0.25 mA cm <sup>-2</sup> and 0.05 mAh cm <sup>-2</sup>	[174]
MTSi-Hedp <sup>[c]</sup> ≈ 264 nm	Homogenize the Zn ion flux; Optimize nucleation barrier	Dip coating	~24.3 mV	over 2000 cycles at 1 mA cm <sup>-2</sup> and 1 mAh cm <sup>-2</sup>	[176]
PA/Zn(TFO) <sub>2</sub>	Optimize nucleation barrier; Uniform electrical field	Blade coating	100 mV	over 8000 h at 0.5 mA cm <sup>-2</sup> and 0.25 mAh cm <sup>-2</sup>	[37]

[a] PA is the abbreviation of polyamide; [b] COP-CMC/QG consists of a covalent organic polymer (COP) and carboxyl methyl cellulose (CMC), is designed to in situ construct a multifunctional quasi gel (COP-CMC/QG) interface between Zn metal and the ZnSO<sub>4</sub> electrolyte; [c] MTSi refers to Methyl triethoxy silane. Hedp refers to hydroxy ethyldene diphosphonic acid.

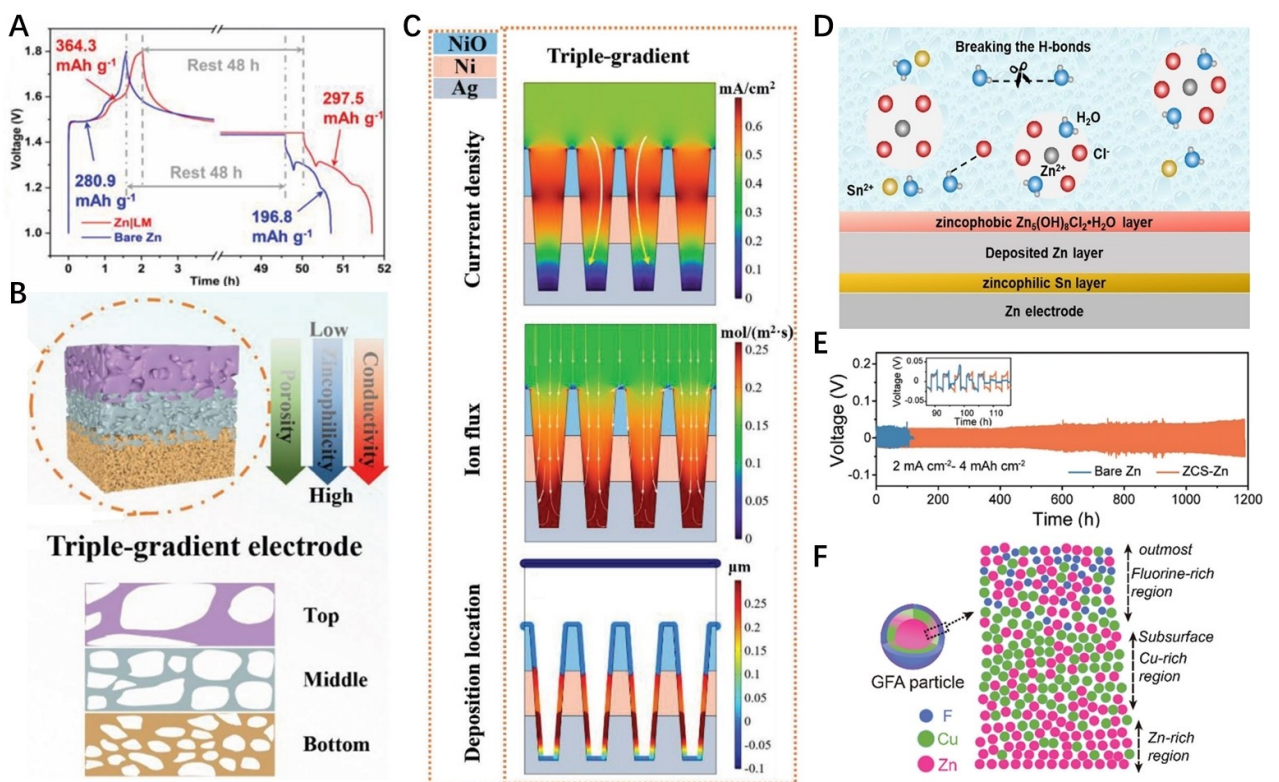


**Figure 10.** A) Voltage-time plots of Zn/LM//MnO<sub>2</sub> full cells at 0.2 A g<sup>-1</sup> in ZnSO<sub>4</sub> electrolyte (fully charged to 1.8 V, rest for 48 h, then fully discharging). LCNF refers to lignin-containing cellulose nanofiber. LM = (LCNF)-Mxene. Reproduced from ref. [167]. Copyright (2022), with permission from Wiley-VCH. B) Schematic diagram for the Ag/NiO triple-gradient electrode. C) The finite element simulations of Ag/NiO triple-gradient electrodes. Current density (up), ion flux (middle) and deposition location distribution (down) Reproduced from ref. [168]. Copyright (2022), with permission from American Chemical Society. D) Scheme of electrolyte and electrolyte-electrode-interphase structure after adding 0.05 m SnCl<sub>2</sub> in 7.6 M ZnCl<sub>2</sub> aqueous electrolyte. Reproduced from ref. [170]. Copyright (2022), with permission from Wiley-VCH. E) The long-term cycling performance of Zn||Zn symmetrical cells protected by Zn<sub>3</sub>(PO<sub>4</sub>)<sub>2</sub> and ZnF<sub>2</sub> (ZCS) layers at 2 mA cm<sup>-2</sup> with 4 mAh cm<sup>-2</sup>. Reproduced from ref. [171]. Copyright (2021), with permission from The Royal Society of Chemistry. F) Illustration of the elemental distribution inside a gradient fluorinated alloying (GFA) composite AIL in ZnSO<sub>4</sub> electrolyte. Reproduced from ref. [173]. Copyright (2022), with permission from The Royal Society of Chemistry.

in the foam electrolyte. The electrochemical impedance spectra (EIS) results exhibit the rapid Zn<sup>2+</sup> transport dynamics and inhibited side reactions at the anode/electrolyte interface in COP-CMC–Zn (Figure 10B). Zn symmetrical battery protected by composite COP-CMC can cycle for more than 4000 hours at 0.25 mA cm<sup>-2</sup>, and even work for 1000 hours at a high current density of 5 mA cm<sup>-2</sup>.

Except for functional quasi-gel layer, hydrophobic siloxane blocks and zincophilic diphosphate building blocks have been integrated into the molecular skeleton on the Zn foil (MTSi-Hedp-Zn) to form a self-consistent ultra-thin multifunctional layer.<sup>[176]</sup> Methyltriethoxysilane (MTSi) rich in O–Si–CH<sub>3</sub> groups was selected to act hydrophobic sites as a hydrophobic donor. Hydroxy ethylidene diphosphonic acid (Hedp) with phosphate group was chosen to form Zincophilicity sites through the formed Zn chelate (Figure 10C). The molecular electrical potential (MESP) distribution was calculated to further confirm that P–O is a highly active center to facilitate Zn<sup>2+</sup> deposition (Figure 10D). The Lowest unoccupied molecular orbital (LUMO) and highest occupied molecular orbital (HOMO) of MTSi-Hedp and MTSi-Hedp were respectively displayed in the Figure 10(E). The energy gap between HOMO and LOMO was represented by E<sub>HOMO-LUMO</sub> which value is inversely proportional to the

electronic conductivity, implying the inherent electronic conductivity of organic hosts and the most excellent electronic conductivity of MTSi-Hedp among MTSi-Hedp, MTSi and Hedp monomer (Figure 10E). This feature is conducive to the uniform and rapid deposition of Zn<sup>2+</sup> on the nano film layer, enabling the MTSi-Hedp-Zn anode to have excellent electrochemical performance in terms of rate ability, reversibility, and recyclability. It can form a strong chelating chain between Zn metal and Hedp, effectively ensuring good adhesion. The zincophilic Zn-Hedp complex formed by the interaction between the phosphate group and the Zn atom on the skeleton can be considered as a zincophilic region attracting the migration of Zn ion and homogeneous ions. When the formed MTSi-Hedp-Zn paired with a V<sub>2</sub>O<sub>5</sub> cathode, the full cell retains an excellent cycle stability with discharge capacity of 103.3 mAh g<sup>-1</sup> at 3 A g<sup>-1</sup> after 2000 cycles.

Zhao et.al fabricated a multifunctional polymeric interphase mainly constituted of Zn(TFO)<sub>2</sub> and cost-effective polyamide (PA) through engineering designed in the AZIBs.<sup>[37]</sup> The artificial PA layer provides at least two ways to inhibit HER and other side reactions (Figure 10F): (1) as a physical buffer layer to inhibit the chaotic aqueous electrolyte and dissolved O<sub>2</sub>; (2) insulating Zn anode from harmful water molecules at the

internal microscopic level by the abundant hydrogen bond networks based on intrinsic amide group in PA and the desolvation when cation passing through the interphase. Based on the above two functions, the symmetrical Zn//Zn cell with the polymeric interphase exhibited stable Zn plating/stripping performance over 2600 h at 1 mAc<sup>-2</sup> with low deposition potentials around 50 mV). Further investigation showed that the surface of PA layer modified Zn anode was dense and free of dendrites whereas the exposed Zn plate showed reversible dendrites after 450 cycles (Figure 10G).

However, this conventional separation battery configuration and the common interface contact limit the high magnification capability and mechanical flexibility of the Zn battery. Chen et al. proposed an ingenious "all-in-one" AZIB with integrated configuration for the stable and flexible energy storage.<sup>[177]</sup> In this precisely designed structure, the PA microporous filter membrane tightly attached to the Zn metal anode. This kind separator has excellent flexibility and is usually used for AZIBs. The internal Zn(TFO)<sub>2</sub>-PA protective coating is located between the Zn anode and the PA separator, which severs as a "glue" to bond the Zn anode and the PA separator together. The "all in one" structure not only facilitates the formation of dendrite-free Zn deposition to ensure the long-term cycle life, but also enhances the interface contact to reduce the battery polarization and afford sufficient magnification capability (Figure 11).

#### 4. Conclusion and outlook

AZIBs have received tremendous research interests for the past decades. and are considered as a promising candidate for next-generation electrochemical energy storage system because of its low cost, good safety, and environmental benignity. Compared to the relatively mature-developed several cathode materials, Zn anodes still faces numerous intractable challenges. The unstable bare Zn anode suffers from low cycling performance and poor CE, which seriously hinders the practical application of AZIBs. Designing a robust and ingenious AIL is a significant prerequisite to achieve stable Zn metal anodes and improved electrochemical performance. Therefore, the composite AILs have been successfully used as a physical isolation barrier, homogenize the Zn<sup>2+</sup> flux, optimize nucleation barrier, uniform electrical field, and regulate Zn<sup>2+</sup> solvation structure on the surface of Zn anodes. The composite AILs are considered the most promising candidate for combining multiple functions from different materials. Although significant progress has been obtained on the effective design of multifunctional composite AILs towards stable Zn metal anode, there are still many challenges that urgently need to be addressed. In this review, we propose several suggestions and perspectives in this field:

The simple and low-cost methods for constructing AILs need to be carried out. The complexity degree and manufacturing cost of the engineering determine the potential for practical applications of composite AILs. Many methods exhibit simplicity and flexibility, such as blade coating, spin coating, drop coating, dip coating, etc. Among the approaches summarized above, the electrolyte additive strategy is the simplest as a burgeoning

techniques and blade coating is the most cost-effective method as a traditional technique. However, the former is usually expensive and the latter is relatively complex. If complex and expensive synthesis methods are used to construct composite AIL, it will violate the low-cost energy storage and conversion of AZIBs. Therefore, it is necessary to consider finding a simple and low-cost synthesis method for composite AILs.

Further development is required for building adaptive, self-healing composite AILs. Although various surface coatings have shown good results in protecting Zn anodes, it should be noted that most coatings undergo significant volume changes during repeated galvanizing/stripping processes, ultimately losing their functionality. Therefore, it is necessary to carefully design a protective layer to improve the performance of Zn anodes by inhibiting Zn dendrite growth and side reactions while maintaining structural integrity. Therefore, self-healing composite AILs can effectively alleviate the structural expansion and reversible Zn plating/stripping to enhance cycle performance. Subsequently, microcells for wearable electronics, and soft package cells for large-scale energy storage stations with cycling stability and long lifespan will be further developed.

There are some conflicting reports on the design principles of composite AILs to Zn anode. For example, some researchers believe that AILs with good hydrophilicity can improve electrode wettability and reduce interface resistance, thereby facilitating uniform flux and nucleation of Zn for uniform Zn deposition. On the contrary, some researchers believe that hydrophobic AILs promote the aggregation of Zn ions, leading to local deposition of Zn in energetically favorable locations. These researchers believe that hydrophobic layers can reduce interfacial side reactions generated by water, which is also an undeniable fact. In addition, when it comes to whether AILs should be zincophilic or zincophobic, there are still different opinions. It has been well established that coatings with high Zn affinity have greater binding energy with Zn atoms. Thus, some researchers considered AIL with high zincophilicity leads to selective adsorption of Zn atoms and even accidental deposition on the coating, causing the formation of dendrites. Nonetheless, some researchers considered AILs with high zincophilicity enables it to easily grab Zn atoms and guide subsequent deposition on the zinc substrate, resulting in a smooth shape and improved cycle performance. We believe that the different viewpoints is closely related to the structure and density of the zincophobic sites in fabricated AILs.

The protect mechanism of composite AILs is waiting to be further explored. For example, the evolution process and electrochemical conversion mechanism of the solvation structure regulated by AILs are still unclear. Zn<sup>2+</sup> shuttles between the negative and positive electrodes in the form of six H<sub>2</sub>O surrounding structure (such as Zn(H<sub>2</sub>O)<sub>6</sub>) in aqueous electrolytes due to their high charge state. The large solvent shell in the electrolyte can cause charge transfer resistance and electrochemical polarization, leading to slow electrochemical reaction kinetics and resultant low power density. Although many studies have focused on constructing AILs that regulate solvation structures to improve electrochemical performance,

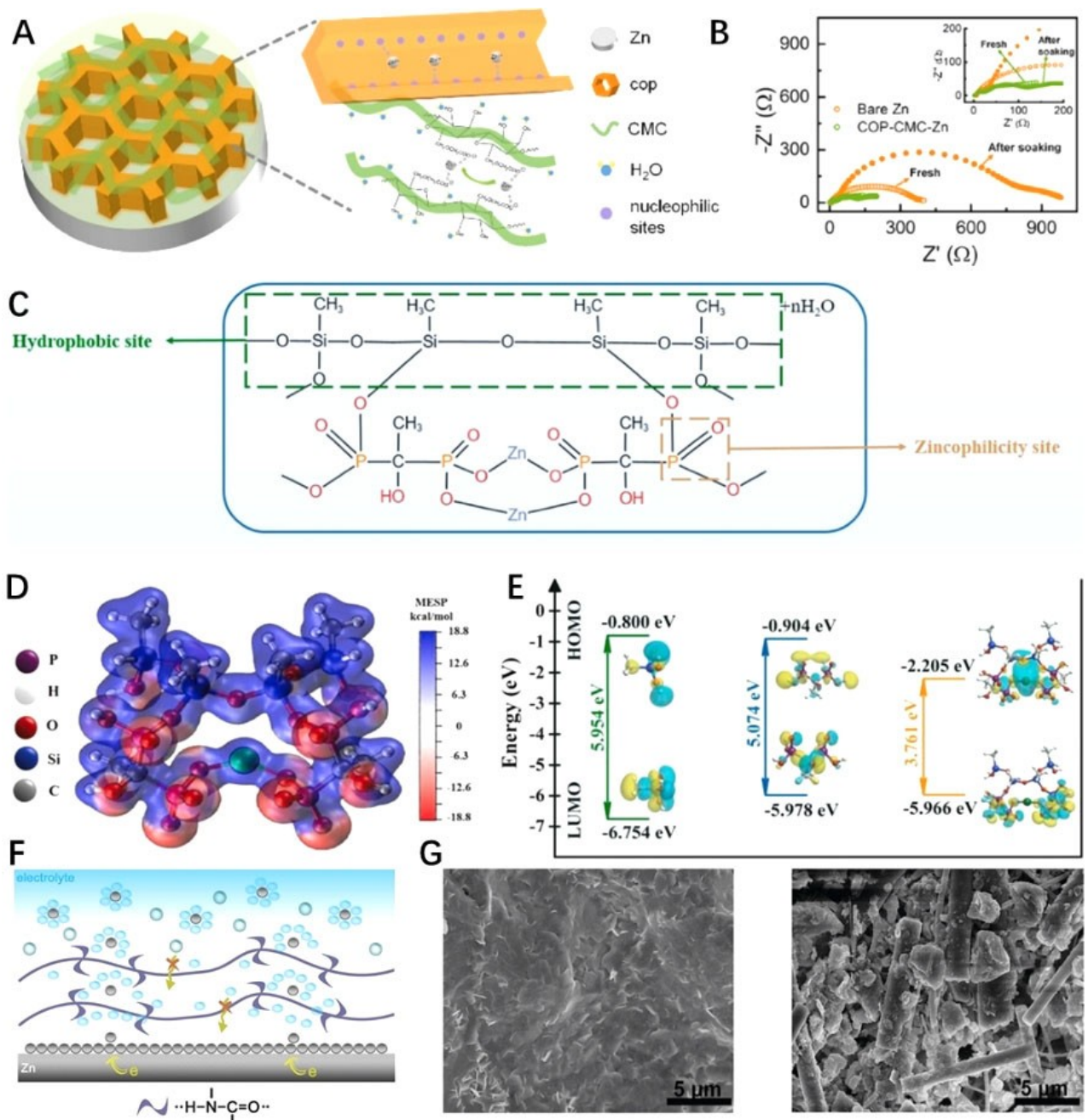


**Figure 11.** A) Schematic diagram of COP-CMC/QG. COP-CMC/QG consists of a covalent organic polymer (COP) and carboxymethyl cellulose (CMC), is designed to in situ construct a multifunctional quasi gel (COP-CMC/QG) interface between Zn metal and the  $\text{ZnSO}_4$  electrolyte. B) EIS curves of bare Zn and COP-CMC-Zn before and after immersing in the  $\text{ZnSO}_4$  electrolyte. Reproduced from ref. [174]. Copyright (2021), with permission from American Chemical Society. C) Schematic of diagram hydrophobic sites and Zincophilicity sites on MTSi-Hedp-Zn. MTsi refers to Methyltriethoxysilane. Hedp refers to hydroxy ethylenediphosphonic acid. D) Calculated frontier molecular orbital energy of MTSi(left), Hedp(middle) and MTSi-Hedp (right). E) Calculated ESP distribution of MTSi-Hedp-Zn. Reproduced from ref. [176]. Copyright (2022), with permission from Elsevier Ltd. F) Schematic diagrams for Zn deposition on the PA/Zn ( $\text{TFO}_2$ ) coated Zn, suggesting the role of the PA layer in the inhibition of side reactions. PA = polyamide. G) SEM images of the surface of the coated Zn plate anode (the PA layer was torn off) after 1000 cycles (left) and the bare Zn plate anode after 450 cycles (right). Reproduced from ref. [37]. Copyright (2022), with permission from The Royal Society of Chemistry.

the theory of the electrochemical conversion mechanism of solvation structures is still immature.

Innovative multifunctional composite AILs are expected to be proposed to achieve dendritic free Zn metal anodes. The ideal AIL shall possess sufficient thermal stability and satisfactory mechanical property. A composite AIL usually composes of

two or more materials combines the advantages of different components to achieve multiple protection for Zn anodes, aiming to realize the high reversibility and dendrites-free Zn growth at the same time. To achieve this ultimate objective, elaborate screening of materials and structure design should be conducted to meet the numerous requirements.

Stable AILs under extreme temperatures urgently need to be designed to broaden applications. Although AZIBs are promising for next-generation energy storage, the grievous Zn dendrite growth at low temperatures and severe parasitic reactions of Zn metal anode at high temperatures greatly restrict the development of wide-temperature AZIBs. It puts higher demands on the development of AILs with superior thermal stability and protective functions. For example, the sluggish transport kinetics of  $Zn^{2+}$  at low temperatures is not conducive to uniform Zn stripping electroplating. By designing multifunctional electrolytes, multiple modulations can be achieved, including lowering the freezing point and forming in situ AILs. To accelerate the sluggish kinetics, future studies should pay more attention to constructing thinner interface layers with high  $Zn^{2+}$  conductivity.

In this review, we have briefly summarized the origin and mechanism of dendrite growth and side reactions; reviewed the five fundamental protection mechanisms of AILs; highlighted the functional orientation design of the materials and structures in composite AILs based on the above five mechanisms towards the suppression of Zn dendrite growth and side reactions generation as well as the resultant improvement of the electrochemical performance of Zn anodes. By this review, we hope to illustrate a comprehensive and timely summarization of the composite AILs according to the materials types, which is not only essential to present full-spectrum research progress but also effective to provide directions for the future research of this promising field.

## Acknowledgements

This work was supported by the Fundamental Research Funds for the Central Universities (N2305010, N232410019), the Natural Science Foundation of Liaoning Province of China (2023-MS-088), the National Natural Science Foundation of China (21773055, 22309073, and U22A20437) and Joint Fund of Science and Technology R&D Plan of Henan Province (222301420005).

## Conflict of Interests

The authors declare no conflict of interest.

**Keywords:** Aqueous Zn ion batteries • Composite artificial interface layers • Zinc anode protection • Zn dendrite • Hydrogen evolution reaction

- [1] Z. Yi, G. Chen, F. Hou, L. Wang, J. Liang, *Adv. Energy Mater.* **2020**, *11*, 2003065.
- [2] Q. Zhang, J. Luan, Y. Tang, X. Ji, H. Wang, *Angew. Chem. Int. Ed. Engl.* **2020**, *59*, 13180–13191.
- [3] V. Mathew, B. Sambandam, S. Kim, S. Kim, S. Park, S. Lee, M. H. Alfaruqi, V. Soundharrajan, S. Islam, D. Y. Putro, J.-Y. Hwang, Y.-K. Sun, J. Kim, *ACS Energy Lett.* **2020**, *5*, 2376–2400.
- [4] Q. Zhang, Y. Su, Z. Shi, X. Yang, J. Sun, *Small* **2022**, *18*, e2203583.
- [5] H. Wang, M. Wang, Y. Tang, *Energy Storage Mater.* **2018**, *13*, 1–7.

- [6] D. Choi, S. Lim, D. Han, *J. Energy Chem.* **2021**, *53*, 396–406.
- [7] B.-E. Jia, A. Q. Thang, C. Yan, C. Liu, C. Lv, Q. Zhu, J. Xu, J. Chen, H. Pan, Q. Yan, *Small* **2022**, *18*, 2107773.
- [8] Y. S. Joe, M. S. Kang, G. Jang, S. J. Lee, P. Nakhanivei, S. H. Baek, Y. K. Kim, G. Jeong, H.-s. Kim, H. S. Park, *Chem. Eng. J.* **2023**, *460*, 141706.
- [9] Y. Chen, D. Ma, S. Shen, P. Deng, Z. Zhao, M. Yang, Y. Wang, H. Mi, P. Zhang, *Energy Storage Mater.* **2023**, *56*, 600–610.
- [10] L. Ma, H. Cui, S. Chen, X. Li, B. Dong, C. Zhi, *Nano Energy* **2021**, *81*, 105632.
- [11] J. Guan, Q. Huang, L. Shao, X. Shi, D. Zhao, L. Wang, Z. Sun, *Small* **2023**, *19*, 2207148.
- [12] Y. Gao, L. Xia, J. Yin, Z. Gan, X. Feng, G. Meng, Y. Cheng, X. Xu, *Small Methods* **2022**, *6*, 2200999.
- [13] R. Zhao, J. Yang, X. Han, Y. Wang, Q. Ni, Z. Hu, C. Wu, Y. Bai, *Adv. Energy Mater.* **2023**, *13*, 2203542.
- [14] Q. Gou, H. Luo, Q. Zhang, J. Deng, R. Zhao, O. Odunmbaku, L. Wang, L. Li, Y. Zheng, J. Li, D. Chao, M. Li, *Small* **2023**, *19*, 2207502.
- [15] W. Zhang, H. L. Zhuang, L. Fan, L. Gao, Y. Lu, *Sci. Adv.* **2018**, *4*, eaar4410.
- [16] J. Cao, D. Zhang, X. Zhang, Z. Zeng, J. Qin, Y. Huang, *Energy Environ. Sci.* **2022**, *15*, 499–528.
- [17] R. Zhang, X.-R. Chen, X. Chen, X.-B. Cheng, X.-Q. Zhang, C. Yan, Q. Zhang, *Angew. Chem. Int. Ed.* **2017**, *56*, 7764–7768.
- [18] Q. Zhao, S. Stalin, L. A. Archer, *Joule* **2021**, *5*, 1119–1142.
- [19] Y. Lee, B. Ma, P. Bai, *Energy Environ. Sci.* **2020**, *13*, 3504–3513.
- [20] S. Guo, L. Qin, T. Zhang, M. Zhou, J. Zhou, G. Fang, S. Liang, *Energy Storage Mater.* **2021**, *34*, 545–562.
- [21] J. Ruan, D. Ma, K. Ouyang, S. Shen, M. Yang, Y. Wang, J. Zhao, H. Mi, P. Zhang, *Nano-Micro Lett.* **2023**, *15*, 37.
- [22] R. Wang, S. Xin, D. Chao, Z. Liu, J. Wan, P. Xiong, Q. Luo, K. Hua, J. Hao, C. Zhang, *Adv. Funct. Mater.* **2022**, *32*, 2207751.
- [23] W. Guo, Z. Cong, Z. Guo, C. Chang, X. Liang, Y. Liu, W. Hu, X. Pu, *Energy Storage Mater.* **2020**, *30*, 104–112.
- [24] R. Yu, H. Zhang, B. Guo, *Nano-Micro Lett.* **2021**, *14*, 1.
- [25] Q. Li, Y. Wang, F. Mo, D. Wang, G. Liang, Y. Zhao, Q. Yang, Z. Huang, C. Zhi, *Adv. Energy Mater.* **2021**, *11*, 2003931.
- [26] R. Zhu, Z. Xiong, H. Yang, N. Wang, S. Kitano, C. Zhu, Y. Aoki, H. Habazaki, *Adv. Funct. Mater.* **2022**, *13*, 2211274.
- [27] M. Wang, W. Wang, Y. Meng, Y. Xu, J. Sun, Y. Yuan, M. Chuai, N. Chen, X. Zheng, R. Luo, K. Xu, W. Chen, *Energy Storage Mater.* **2023**, *56*, 424–431.
- [28] Y. Liu, S. Liu, X. Xie, Z. Li, P. Wang, B. Lu, S. Liang, Y. Tang, J. Zhou, *InfoMat* **2022**, *5*, e12374.
- [29] C. Li, Z. Sun, T. Yang, L. Yu, N. Wei, Z. Tian, J. Cai, J. Lv, Y. Shao, M. H. Rümmeli, J. Sun, Z. Liu, *Adv. Mater.* **2020**, *32*, 2003425.
- [30] J. Han, H. Euchner, M. Kuenzel, S. M. Hosseini, A. Groß, A. Varzi, S. Passerini, *ACS Energy Lett.* **2021**, *6*, 3063–3071.
- [31] Z. Wang, H. Chen, H. Wang, W. Huang, H. Li, F. Pan, *ACS Energy Lett.* **2022**, *7*, 4168–4176.
- [32] X. Feng, P. Li, J. Yin, Z. Gan, Y. Gao, M. Li, Y. Cheng, X. Xu, Y. Su, S. Ding, *ACS Energy Lett.* **2023**, *8*, 1192–1200.
- [33] S.-J. Zhang, J. Hao, D. Luo, P.-F. Zhang, B. Zhang, K. Davey, Z. Lin, S.-Z. Qiao, *Adv. Energy Mater.* **2021**, *11*, 2102010.
- [34] M. Li, X. Wang, J. Hu, J. Zhu, C. Niu, H. Zhang, C. Li, B. Wu, C. Han, L. Mai, *Angew. Chem. Int. Ed.* **2023**, *62*, e202215552.
- [35] Y. Xie, J. Huang, T. Kong, X. Zhou, K. Wu, X. Liu, J. Yi, L. Xing, Y. Xia, *Energy Storage Mater.* **2023**, *56*, 218–226.
- [36] L. Ma, S. Chen, X. Li, A. Chen, B. Dong, C. Zhi, *Angew. Chem. Int. Ed.* **2020**, *59*, 23836–23844.
- [37] Z. Zhao, J. Zhao, Z. Hu, J. Li, J. Li, Y. Zhang, C. Wang, G. Cui, *Energy Environ. Sci.* **2019**, *12*, 1938–1949.
- [38] J. Yang, R. Zhao, Y. Wang, Z. Hu, Y. Wang, A. Zhang, C. Wu, Y. Bai, *Adv. Funct. Mater.* **2023**, *33*, 2213510.
- [39] X. Zeng, J. Mao, J. Hao, J. Liu, S. Liu, Z. Wang, Y. Wang, S. Zhang, T. Zheng, J. Liu, P. Rao, Z. Guo, *Adv. Mater.* **2021**, *33*, 2007416.
- [40] J. Nai, X. Zhao, H. Yuan, X. Tao, L. Guo, *Nano Res.* **2021**, *14*, 2053–2066.
- [41] D. Li, L. Cao, T. Deng, S. Liu, C. Wang, *Angew. Chem. Int. Ed.* **2021**, *60*, 13035–13041.
- [42] S. Zhai, X. Shi, K. Jiang, X. Tan, W. Zhang, J. Zhang, H. Zhang, Z. Li, *Chem. Eng. J.* **2022**, *437*, 135246.
- [43] R. Li, M. Li, X. Wu, H. Yu, R. Jin, J. Liang, *Mater. Des.* **2023**, *225*, 111583.
- [44] Y. Li, P. Wu, W. Zhong, C. Xie, Y. Xie, Q. Zhang, D. Sun, Y. Tang, H. Wang, *Energy Environ. Sci.* **2021**, *14*, 5563–5571.
- [45] D. Han, S. Wu, S. Zhang, Y. Deng, C. Cui, L. Zhang, Y. Long, H. Li, Y. Tao, Z. Weng, Q.-H. Yang, F. Kang, *Small* **2020**, *16*, 2001736.

- [46] L. Hong, L.-Y. Wang, Y. Wang, X. Wu, W. Huang, Y. Zhou, K.-X. Wang, J.-S. Chen, *Adv. Sci.* **2022**, *9*, 2104866.
- [47] J. Hao, B. Li, X. Li, X. Zeng, S. Zhang, F. Yang, S. Liu, D. Li, C. Wu, Z. Guo, *Adv. Mater.* **2020**, *32*, 2003021.
- [48] M. Wang, Y. Meng, K. Li, T. Ahmad, N. Chen, Y. Xu, J. Sun, M. Chuai, X. Zheng, Y. Yuan, C. Shen, Z. Zhang, W. Chen, *eScience* **2022**, *2*, 509–517.
- [49] Z. Li, L. Wu, S. Dong, T. Xu, S. Li, Y. An, J. Jiang, X. Zhang, *Adv. Funct. Mater.* **2021**, *31*, 2006495.
- [50] J. Zhou, M. Xie, F. Wu, Y. Mei, Y. Hao, R. Huang, G. Wei, A. Liu, L. Li, R. Chen, *Adv. Mater.* **2021**, *33*, 2101649.
- [51] C. Shen, X. Li, N. Li, K. Xie, J.-g. Wang, X. Liu, B. Wei, *ACS Appl. Mater. Interfaces* **2018**, *10*, 25446–25453.
- [52] M. Li, Q. He, Z. Li, Q. Li, Y. Zhang, J. Meng, X. Liu, S. Li, B. Wu, L. Chen, Z. Liu, W. Luo, C. Han, L. Mai, *Adv. Energy Mater.* **2019**, *9*, 1901469.
- [53] J. Dong, H. Peng, J. Wang, C. Wang, D. Wang, N. Wang, W. Fan, X. Jiang, J. Yang, Y. Qian, *Energy Storage Mater.* **2023**, *54*, 875–884.
- [54] X. Chen, W. Li, S. Hu, N. G. Akhmedov, D. Reed, X. Li, X. Liu, *Nano Energy* **2022**, *98*, 107269.
- [55] H. Yang, Z. Chang, Y. Qiao, H. Deng, X. Mu, P. He, H. Zhou, *Angew. Chem. Int. Ed.* **2020**, *59*, 9377–9381.
- [56] S. Wei, Z.-H. Qi, Y. Xia, S. Chen, C. Wang, Y. Wang, P. Zhang, K. Zhu, Y. Cao, X. Guo, X. Yang, Q. Cui, X. Liu, X. Wu, L. Song, *ACS Nano* **2022**, *16*, 21152–21162.
- [57] C. Guo, J. Zhou, Y. Chen, H. Zhuang, J. Li, J. Huang, Y. Zhang, Y. Chen, S.-L. Li, Y.-Q. Lan, *Angew. Chem. Int. Ed.* **2023**, *62*, e202300125.
- [58] J. Cao, D. Zhang, X. Zhang, M. Sawangphruk, J. Qin, R. Liu, *J. Mater. Chem. A* **2020**, *8*, 9331–9344.
- [59] J. Feng, D. Ma, K. Ouyang, M. Yang, Y. Wang, J. Qiu, T. Chen, J. Zhao, B. Yong, Y. Xie, H. Mi, L. Sun, C. He, P. Zhang, *Adv. Funct. Mater.* **2022**, *32*, 2207909.
- [60] S. Yang, Y. Li, H. Du, Y. Liu, Y. Xiang, L. Xiong, X. Wu, X. Wu, *ACS Sustainable Chem. Eng.* **2022**, *10*, 12630–12641.
- [61] Y. Yang, C. Liu, Z. Lv, H. Yang, Y. Zhang, M. Ye, L. Chen, J. Zhao, C. Li, *Adv. Mater.* **2021**, *33*, 2007388.
- [62] P. X. Sun, Z. Cao, Y. X. Zeng, W. W. Xie, N. W. Li, D. Luan, S. Yang, L. Yu, X. W. Lou, *Angew. Chem. Int. Ed.* **2022**, *61*, e202115649.
- [63] P. Cao, H. Zhou, X. Zhou, Q. Du, J. Tang, J. Yang, *ACS Sustainable Chem. Eng.* **2022**, *10*, 8350–8359.
- [64] K. Lu, C. Chen, Y. Wu, C. Liu, J. Song, H. Jing, P. Zhao, B. Liu, M. Xia, Q. Hao, W. Lei, *Chem. Eng. J.* **2023**, *457*, 141287.
- [65] Z. Liu, J. Ren, F. Wang, X. Liu, Q. Zhang, J. Liu, P. Kaghazchi, D. Ma, Z. Chi, L. Wang, *ACS Appl. Mater. Interfaces* **2021**, *13*, 27085–27095.
- [66] R. Qin, Y. Wang, L. Yao, L. Yang, Q. Zhao, S. Ding, L. Liu, F. Pan, *Nano Energy* **2022**, *98*, 107333.
- [67] R. N. Wasalathantri, R. Akolkar, *J. Electrochem. Soc.* **2022**, *169*, 092519.
- [68] N. A. Thieu, W. Li, X. Chen, S. Hu, H. Tian, H. N. N. Tran, W. Li, D. M. Reed, X. Li, X. Liu, *Batteries* **2023**, 9,41.
- [69] M. Zhu, Q. Ran, H. Huang, Y. Xie, M. Zhong, G. Lu, F.-Q. Bai, X.-Y. Lang, X. Jia, D. Chao, *Nano-Micro Lett.* **2022**, *14*, 219.
- [70] Q. Zhang, J. Luan, X. Huang, L. Zhu, Y. Tang, X. Ji, H. Wang, *Small* **2020**, *16*, 2000929.
- [71] D. Li, J. Chen, Y. Chen, Y. Wang, Y. Fu, M. Shao, Z. Shi, *J. Energy Chem.* **2023**, *78*, 169–177.
- [72] M. Tomellini, *Physica A* **2018**, *496*, 481–494.
- [73] V. A. Isaev, O. V. Grishenkova, Y. P. Zaykov, *J. Electrochem. Soc.* **2018**, *818*, 265–269.
- [74] L. Wang, W. Huang, W. Guo, Z. H. Guo, C. Chang, L. Gao, X. Pu, *Adv. Funct. Mater.* **2022**, *32*, 2108533.
- [75] J. Yang, R. Zhao, Y. Wang, Z. Hu, Y. Wang, A. Zhang, C. Wu, Y. Bai, *Adv. Funct. Mater.* **2023**, *33*, 2213510.
- [76] Y. Guo, X. Li, H. Guo, Q. Qin, Z. Wang, J. Wang, G. Yan, *Energy Storage Mater.* **2022**, *51*, 476–485.
- [77] Y. Zhou, G. Li, S. Feng, H. Qin, Q. Wang, F. Shen, P. Liu, Y. Huang, H. He, *Adv. Sci.* **2022**, *10*, 2205874.
- [78] D. Zalka, L. Péter, *J. Solid State Electrochem.* **2020**, *24*, 2595–2602.
- [79] C. Xie, S. Liu, Z. Yang, H. Ji, S. Zhou, H. Wu, C. Hu, Y. Tang, X. Ji, Q. Zhang, H. Wang, *Angew. Chem. Int. Ed.* **2023**, *62*, e202218612.
- [80] H. Chen, Z. Guo, H. Wang, W. Huang, F. Pan, Z. Wang, *Energy Storage Mater.* **2023**, *54*, 563–569.
- [81] L. Hu, P. Xiao, L. Xue, H. Li, T. Zhai, *EnergyChem* **2021**, *3*, 100052.
- [82] C. Xie, Y. Li, Q. Wang, D. Sun, Y. Tang, H. Wang, *Carbon Energy* **2020**, *2*, 540–560.
- [83] B. Sambandam, V. Mathew, S. Kim, S. Lee, S. Kim, J. Y. Hwang, H. J. Fan, J. Kim, *Chem* **2022**, *8*, 924–946.
- [84] J. Hao, X. Li, S. Zhang, F. Yang, X. Zeng, S. Zhang, G. Bo, C. Wang, Z. Guo, *J. Mater. Chem. A* **2020**, *30*, 2001263.
- [85] R. Sun, D. Han, C. Cui, Z. Han, X. Guo, B. Zhang, Y. Guo, Y. Liu, Z. Weng, Q.-H. Yang, *Angew. Chem. Int. Ed.* **2023**, *62*, e202303557.
- [86] P. Xue, C. Guo, N. Wang, K. Zhu, S. Jing, S. Kong, X. Zhang, L. Li, H. Li, Y. Feng, W. Gong, Q. Li, *Adv. Funct. Mater.* **2021**, *31*, 2106417.
- [87] Y. Lv, Y. Xiao, L. Ma, C. Zhi, S. Chen, *Adv. Mater.* **2022**, *34*, 2106409.
- [88] Y. Yang, H. Hua, Z. Lv, M. Zhang, C. Liu, Z. Wen, H. Xie, W. He, J. Zhao, C. C. Li, *Adv. Funct. Mater.* **2023**, *33*, 2212446.
- [89] Q. Lu, C. Liu, Y. Du, X. Wang, L. Ding, A. Omar, D. Mikhailova, *ACS Appl. Mater. Interfaces* **2021**, *13*, 16869–16875.
- [90] Y. Bai, H. Zhang, M. Usman Tahir, B. Xiang, *J. Colloid Interface Sci.* **2022**, *608*, 22–29.
- [91] S. Jiao, J. Fu, M. Wu, T. Hua, H. Hu, *ACS Nano* **2022**, *16*, 1013–1024.
- [92] Q. Zhang, Y. Ma, Y. Lu, X. Zhou, L. Lin, L. Li, Z. Yan, Q. Zhao, K. Zhang, J. Chen, *Angew. Chem. Int. Ed.* **2021**, *60*, 23357–23364.
- [93] S. D. Pu, B. Hu, Z. Li, Y. Yuan, C. Gong, Z. Ning, C. Chau, S. Yang, S. Zhang, L. Pi, Y. T. Tang, J. Yue, T. J. Marrow, X. Gao, P. G. Bruce, A. W. Robertson, *Joule* **2023**, *7*, 366–379.
- [94] X. Zeng, K. Xie, S. Liu, S. Zhang, J. Hao, J. Liu, W. K. Pang, J. Liu, P. Rao, Q. Wang, J. Mao, Z. Guo, *Energy Environ. Sci.* **2021**, *14*, 5947–5957.
- [95] Z. Cao, X. Zhu, D. Xu, P. Dong, M. O. L. Chee, X. Li, K. Zhu, M. Ye, J. Shen, *Energy Storage Mater.* **2021**, *36*, 132–138.
- [96] M. Liu, L. Yang, H. Liu, A. Amine, Q. Zhao, Y. Song, J. Yang, K. Wang, F. Pan, *ACS Appl. Mater. Interfaces* **2019**, *11*, 32046–32051.
- [97] J. Zhou, L. Zhang, M. Peng, X. Zhou, Y. Cao, J. Liu, X. Shen, C. Yan, T. Qian, *Adv. Mater.* **2022**, *34*, 2200131.
- [98] Y. Su, B. Liu, Q. Zhang, J. Peng, C. Wei, S. Li, W. Li, Z. Xue, X. Yang, J. Sun, *Adv. Funct. Mater.* **2022**, *32*, 2204306.
- [99] H. Liu, Q. Ye, D. Lei, Z. Hou, W. Hua, Y. Huyan, N. Li, C. Wei, F. Kang, J.-G. Wang, *Energy Environ. Sci.* **2023**, *16*, 1610–1619.
- [100] P. Li, J. Ren, C. Li, J. Li, K. Zhang, T. Wu, B. Li, L. Wang, *Chem. Eng. J.* **2023**, *451*, 138769.
- [101] H. Sun, Y. Huyan, N. Li, D. Lei, H. Liu, W. Hua, C. Wei, F. Kang, J.-G. Wang, *Nano Lett.* **2023**, *23*, 1726–1734.
- [102] J. Yan, M. Ye, Y. Zhang, Y. Tang, C. Chao Li, *Chem. Eng. J.* **2022**, *432*, 134227.
- [103] L. Zhou, F. Yang, S. Zeng, X. Gao, X. Liu, X. Cao, P. Yu, X. Lu, *Adv. Funct. Mater.* **2022**, *32*, 2110829.
- [104] H. Jia, M. Qiu, C. Lan, H. Liu, M. Dirican, S. Fu, X. Zhang, *Adv. Sci.* **2022**, *9*, 2103952.
- [105] J. Guo, W. Zhang, J. Yin, Y. Zhu, Z. O. F. Mohammed, H. N. Alshareef, *Energy Technol.-Ger.* **2021**, *9*, 2100490.
- [106] S. Li, J. Fu, G. Miao, S. Wang, W. Zhao, Z. Wu, Y. Zhang, X. Yang, *Adv. Mater.* **2021**, *33*, 2008424.
- [107] C. Wu, K. Xie, K. Ren, S. Yang, Q. Wang, *Dalton* **2020**, *49*, 17629–17634.
- [108] Y. Liu, J. Hu, Q. Lu, M. Hantusch, H. Zhang, Z. Qu, H. Tang, H. Dong, O. G. Schmidt, R. Holze, M. Zhu, *Energy Storage Mater.* **2022**, *47*, 98–104.
- [109] H. Wang, H. Li, Y. Tang, Z. Xu, K. Wang, Q. Li, B. He, Y. Liu, M. Ge, S. Chen, T. Hao, G. Xing, Y. Zhang, *Adv. Funct. Mater.* **2022**, *32*, 2207898.
- [110] Z. Hong, Z. Ahmad, V. Viswanathan, *ACS Energy Lett.* **2020**, *5*, 2466–2474.
- [111] H. Wu, W. Yan, Y. Xing, L. Li, J. Liu, L. Li, P. Huang, C. Lai, C. Wang, W. Chen, S. Chou, *Adv. Funct. Mater.* **2023**, *n/a*, 2213882.
- [112] K. Wu, J. Yi, X. Liu, Y. Sun, J. Cui, Y. Xie, Y. Liu, Y. Xia, J. Zhang, *Nano-Micro Lett.* **2021**, *13*, 79.
- [113] Q. Jian, T. Wang, J. Sun, M. Wu, T. Zhao, *Energy Storage Mater.* **2022**, *53*, 559–568.
- [114] X. Li, X. Wang, L. Ma, W. Huang, *Adv. Energy Mater.* **2022**, *12*, 2202068.
- [115] Z. Cai, Y. Ou, J. Wang, R. Xiao, L. Fu, Z. Yuan, R. Zhan, Y. Sun, *Energy Storage Mater.* **2020**, *27*, 205–211.
- [116] K. Zhao, C. Wang, Y. Yu, M. Yan, Q. Wei, P. He, Y. Dong, Z. Zhang, X. Wang, L. Mai, *Adv. Mater. Interfaces* **2018**, *5*, 1800848.
- [117] H. He, J. Liu, *J. Mater. Chem. A* **2020**, *8*, 22100–22110.
- [118] L. Zeng, J. He, C. Yang, D. Luo, H. Yu, H. He, C. Zhang, *Energy Storage Mater.* **2023**, *54*, 469–477.
- [119] L. Zeng, H. He, H. Chen, D. Luo, J. He, C. Zhang, *Adv. Energy Mater.* **2022**, *12*, 2103708.
- [120] H. Peng, C. Liu, N. Wang, C. Wang, D. Wang, Y. Li, B. Chen, J. Yang, Y. Qian, *Energy Environ. Sci.* **2022**, *15*, 1682–1693.
- [121] Y. Wang, Y. Fan, D. Liao, Y. Wu, Y. Yu, C. Hu, *Energy Storage Mater.* **2022**, *51*, 212–222.
- [122] Z. Wang, L. Dong, W. Huang, H. Jia, Q. Zhao, Y. Wang, B. Fei, F. Pan, *Nano-Micro Lett.* **2021**, *13*, 73.

- [123] Q. Zhang, J. Luan, X. Huang, L. Zhu, Y. Tang, X. Ji, H. Wang, *Small* **2020**, 16, 2000929.
- [124] Y. Zeng, X. Zhang, R. Qin, X. Liu, P. Fang, D. Zheng, Y. Tong, X. Lu, *Adv. Mater.* **2019**, 31, 1903675.
- [125] S. Zhou, Y. Wang, H. Lu, Y. Zhang, C. Fu, I. Usman, Z. Liu, M. Feng, G. Fang, X. Cao, S. Liang, A. Pan, *Adv. Funct. Mater.* **2021**, 31.
- [126] J. Cao, D. Zhang, C. Gu, X. Zhang, M. Okhwailai, S. Wang, J. Han, J. Qin, Y. Huang, *Nano Energy* **2021**, 89, 106322.
- [127] A. Chen, C. Zhao, J. Gao, Z. Guo, X. Lu, J. Zhang, Z. Liu, M. Wang, N. Liu, L. Fan, Y. Zhang, N. Zhang, *Energy Environ. Sci.* **2023**, 16, 275–284.
- [128] P. Ye, X. Li, K. He, A. Dou, X. Wang, A. Naveed, Y. Zhou, M. Su, P. Zhang, Y. Liu, *J. Power Sources* **2023**, 558, 232622.
- [129] D. Xie, Z.-W. Wang, Z.-Y. Gu, W.-Y. Diao, F.-Y. Tao, C. Liu, H.-Z. Sun, X.-L. Wu, J.-W. Wang, J.-P. Zhang, *Adv. Funct. Mater.* **2022**, 32, 2204066.
- [130] S. Jin, P.-Y. Chen, Y. Qiu, Z. Zhang, S. Hong, Y. L. Joo, R. Yang, L. A. Archer, *J. Am. Chem. Soc.* **2022**, 144, 19344–19352.
- [131] X. Li, Q. Li, Y. Hou, Q. Yang, Z. Chen, Z. Huang, G. Liang, Y. Zhao, L. Ma, M. Li, Q. Huang, C. Zhi, *ACS Nano* **2021**, 15, 14631–14642.
- [132] A. Feng, Y. Yu, Y. Wang, F. Jiang, Y. Yu, L. Mi, L. Song, *Mater. Des.* **2017**, 114, 161–166.
- [133] J. Liu, J. Zhang, *Chem. Rev.* **2020**, 120, 2123–2170.
- [134] P. Zhang, Y. Peng, Q. Zhu, R. A. Soomro, N. Sun, B. Xu, *Energy Environ. Mater.* **2023**, <https://doi.org/10.1002/eem2.12379>.
- [135] Q. Zhu, J. Li, P. Simon, B. Xu, *Energy Storage Mater.* **2021**, 35, 630–660.
- [136] N. Wang, Z. Wu, Y. Long, D. Chen, C. Geng, X. Liu, D. Han, J. Zhang, Y. Tao, Q.-H. Yang, *J. Energy Chem.* **2022**, 73, 277–284.
- [137] Y. Zhang, Z. Cao, S. Liu, Z. Du, Y. Cui, J. Gu, Y. Shi, B. Li, S. Yang, *Adv. Energy Mater.* **2022**, 12, 2103979.
- [138] H. Gan, J. Wu, R. Li, B. Huang, H. Liu, *Energy Storage Mater.* **2022**, 47, 602–610.
- [139] M.-C. Liu, C.-Y. Tian, D.-T. Zhang, Y.-S. Zhang, B.-M. Zhang, Y.-Y. Wang, C.-Y. Li, M.-J. Liu, B. Gu, K. Zhao, L.-B. Kong, Y.-L. Chueh, *Nano Energy* **2022**, 103, 107805.
- [140] J. Matusik, A. Koteja-Kunecka, P. Maziarz, A. Kunecka, *Chem. Eng. J.* **2022**, 428, 130848.
- [141] X. Liu, Q. Ma, M. Shi, Q. Han, C. Liu, *Chem. Eng. J.* **2023**, 456, 141016.
- [142] W. Qin, H. Liu, J. An, X. Wen, *J. Power Sources* **2020**, 479, 229090.
- [143] S. Wang, Y. Yang, W. Quan, Y. Hong, Z. Zhang, Z. Tang, J. Li, *Nano Energy* **2017**, 32, 294–301.
- [144] Y. Zhao, S. Nong, C. Dong, M. Chen, S. Liang, M. Cai, F. Huang, *ACS Appl. Energ. Mater.* **2022**, 5, 1305–1312.
- [145] Z. Guo, L. Fan, C. Zhao, A. Chen, N. Liu, Y. Zhang, N. Zhang, *Adv. Mater.* **2022**, 34, e2105133.
- [146] E. Kim, I. Choi, K. W. Nam, *Electrochim. Acta* **2022**, 425, 140648.
- [147] H. Fan, M. Li, E. Wang, *Nano Energy* **2022**, 103, 107751.
- [148] H. Qiu, X. Du, J. Zhao, Y. Wang, J. Ju, Z. Chen, Z. Hu, D. Yan, X. Zhou, G. Cui, *Nat. Commun.* **2019**, 10, 5374.
- [149] C. Meng, W.-D. He, H. Tan, X.-L. Wu, H. Liu, J.-J. Wang, *Energy Environ. Sci.* **2023**, 16, 3587–3599.
- [150] Q. He, G. Fang, Z. Chang, Y. Zhang, S. Zhou, M. Zhou, S. Chai, Y. Zhong, G. Cao, S. Liang, A. Pan, *Nano-Micro Lett.* **2022**, 14, 93.
- [151] S. Di, X. Nie, G. Ma, W. Yuan, Y. Wang, Y. Liu, S. Shen, N. Zhang, *Energy Storage Mater.* **2021**, 43, 375–382.
- [152] N. Wang, Y. Zhang, J. Yuan, L. Hu, M. Sun, Z. Li, X. Yao, X. Weng, C. Jia, *ACS Appl. Mater. Interfaces* **2022**, 14, 48081–48090.
- [153] Y.-X. Song, J. Wang, X.-B. Zhong, K. Wang, Y.-H. Zhang, H.-T. Liu, L.-X. Zhang, J.-F. Liang, R. Wen, *Energy Storage Mater.* **2023**, 58, 85–93.
- [154] G. Ma, L. Miao, Y. Dong, W. Yuan, X. Nie, S. Di, Y. Wang, L. Wang, N. Zhang, *Energy Storage Mater.* **2022**, 47, 203–210.
- [155] L. Cao, D. Li, T. Pollard, T. Deng, B. Zhang, C. Yang, L. Chen, J. Vatamanu, E. Hu, M. J. Hourwitz, L. Ma, M. Ding, Q. Li, S. Hou, K. Gaskell, J. T. Fourkas, X. Q. Yang, K. Xu, O. Borodin, C. Wang, *Nat. Nanotechnol.* **2021**, 16, 902–910.
- [156] C. Wu, C. Sun, K. Ren, F. Yang, Y. Du, X. Gu, Q. Wang, C. Lai, *Chem. Eng. J.* **2023**, 452, 139465.
- [157] L. Geng, J. Meng, X. Wang, C. Han, K. Han, Z. Xiao, M. Huang, P. Xu, L. Zhang, L. Zhou, L. Mai, *Angew. Chem. Int. Ed.* **2022**, 61, e202206717.
- [158] S. Wang, Y. Ying, S. Chen, H. Wang, K. K. K. Cheung, C. Peng, H. Huang, L. Ma, J. A. Zapien, *Energy Storage Mater.* **2023**, 63, 102971.
- [159] P. Qing, Z. Wu, Y. Chen, F. Tang, H. Yang, L. Chen, *J. Energy Chem.* **2022**, 72, 149–157.
- [160] B. Sun, P. Wang, L. Yang, X. Wei, Y. Jin, H. Wu, *ACS Appl. Mater. Interfaces* **2022**, 14, 954–960.
- [161] H. Wang, Y. Chen, H. Yu, W. Liu, G. Kuang, L. Mei, Z. Wu, W. Wei, X. Ji, B. Qu, L. Chen, *Adv. Funct. Mater.* **2022**, 32, 2205600.
- [162] X. Li, Z. Liu, J. Li, H. Lei, W. Zhuo, W. Qin, X. Cai, K. N. Hui, L. Pan, W. Mai, *J. Energy Chem.* **2021**, 53, 56–62.
- [163] Y. Zhang, Q. Wang, S. Bi, M. Yao, F. Wan, Z. Niu, *Nanoscale* **2019**, 11, 17630–17636.
- [164] G. Chen, Z. Sang, J. Cheng, S. Tan, Z. Yi, X. Zhang, W. Si, Y. Yin, J. Liang, F. Hou, *Energy Storage Mater.* **2022**, 50, 589–597.
- [165] J. Zheng, Y. Wu, H. Xie, Y. Zeng, W. Liu, A. N. Gandi, Z. Qi, Z. Wang, H. Liang, *ACS Nano* **2023**, 17, 337–345.
- [166] D. Wang, D. Lv, H. Peng, N. Wang, H. Liu, J. Yang, Y. Qian, *Nano Lett.* **2022**, 22, 1750–1758.
- [167] C. Liu, Z. Li, X. Zhang, W. Xu, W. Chen, K. Zhao, Y. Wang, S. Hong, Q. Wu, M. C. Li, C. Mei, *Adv. Sci.* **2022**, 9, e2202380.
- [168] Y. Gao, Q. Cao, J. Pu, X. Zhao, G. Fu, J. Chen, Y. Wang, C. Guan, *Adv. Mater.* **2023**, 35, e2207573.
- [169] L. Cao, D. Li, E. Hu, J. Xu, T. Deng, L. Ma, Y. Wang, X. Q. Yang, C. Wang, *J. Am. Chem. Soc.* **2020**, 142, 21404–21409.
- [170] L. Cao, D. Li, F. A. Soto, V. Ponce, B. Zhang, L. Ma, T. Deng, J. M. Seminario, E. Hu, X. Q. Yang, P. B. Balbuena, C. Wang, *Angew. Chem. Int. Ed. Engl.* **2021**, 60, 18845–18851.
- [171] Y. Chu, S. Zhang, S. Wu, Z. Hu, G. Cui, J. Luo, *Energy Environ. Sci.* **2021**, 14, 3609–3620.
- [172] Y. Mu, T. Zhou, D. Li, W. Liu, P. Jiang, L. Chen, H. Zhou, G. Ge, *Chem. Eng. J.* **2022**, 430, 132839.
- [173] G. Liang, J. Zhu, B. Yan, Q. Li, A. Chen, Z. Chen, X. Wang, B. Xiong, J. Fan, J. Xu, C. Zhi, *Energy Environ. Sci.* **2022**, 15, 1086–1096.
- [174] J. Ding, Y. Liu, S. Huang, X. Wang, J. Yang, L. Wang, M. Xue, X. Zhang, J. Chen, *ACS Appl. Mater. Interfaces* **2021**, 13, 29746–29754.
- [175] Z. Wang, T. Huang, A. Yu, *J. Power Sources* **2021**, 489, 229530.
- [176] H. Yu, Y. Chen, H. Wang, X. Ni, W. Wei, X. Ji, L. Chen, *Nano Energy* **2022**, 99, 107426.
- [177] P. Chen, W. Zhou, Z. Xiao, S. Li, Z. Wang, Y. Wang, S. Xie, *Nano Energy* **2020**, 74, 104905.

Manuscript received: September 20, 2023

Revised manuscript received: November 11, 2023

Accepted manuscript online: November 13, 2023

Version of record online: December 7, 2023